GEAP-4300
Informal Research
and Development Report
July 1963

SODIUM-COOLED REACTORS PROGRAM

FAST CERAMIC REACTOR DEVELOPMENT PROGRAM

Seventh Quarterly Report

April - June, 1963

Prepared for the
United States Atomic Energy Commission
Under
Contract No. AT(04-3)-189, Project Agreement No. 10

Printed in the U. S. A. [redacted]. Available from the Office of Technical Information, Department of Commerce, Washington 25, D. C.

ATOMIC POWER EQUIPMENT DEPARTMENT
GENERAL ELECTRIC
SAN JOSE, CALIFORNIA

GEAP-4300
Informal Research
and Development Report

EDITED BY:

F. J. Leitz, Deputy Project Engineer
Fast Ceramic Reactor Program

APPROVED:

K. P. Cohen, Project Engineer
Fast Ceramic Reactor Program

TABLE OF CONTENTS

LIST OF ILLUSTRATIONS

LIST OF TABLES

SECTION I

INTRODUCTION

The Fast Ceramic Reactor Development Program is an integrated analytical and experimental program directed toward the development of fast reactors employing ceramic fuels, with particular attention to mixed plutonium-uranium oxide. Its major objectives are:

a. Development of a reliable, high performance fast reactor having nuclear characteristics which provide stable and safe operation, and

b. Demonstration of low fuel cycle cost capability for such a reactor, primarily through achieving high burnup of ceramic fuels operating at high specific power.

Progress during the period April 1 - June 30, 1963 on the currently active tasks of this program is described in subsequent sections.

This is the seventh in a series of quarterly progress reports written in partial fulfillment of Contract AT(04-3)-189, Project Agreement No. 10, between the United States Atomic Energy Commission and the General Electric Company. Prior progress reports to the Commission under this contract include the following:

Monthly Progress Letters, Nos. 1-43, from July 1959 through May 1963.

GEAP-3888 FCR Development Program - First Quarterly Report, October - December, 1961.

GEAP-3957 FCR Development Program - Second Quarterly Report, January - March, 1962

GEAP-3981 FCR Development Program - Third Quarterly Report, April - June, 1962.

GEAP-4080 FCR Development Program - Fourth Quarterly Report, July - September, 1962.

GEAP-4158 FCR Development Program - Fifth Quarterly Report, October - December, 1962.

GEAP-4214 FCR Development Program - Sixth Quarterly Report, January - March, 1963.

Supplementary Progress Letters, Nos. 1-6 from October 1962 through May 1963.
Reports from G. D. Collins and W. J. Ozeroff on assignment to CEA-France.

In addition, the following topical reports have been issued:

GEAP-3287 Fast Oxide Breeder - Reactor Physics, Part I - Parametric Study of 300 MWe Reactor Core, P. Greebler, P. Aline, J. Sueoka; November 10, 1959.

GEAP-3347 Fast Oxide Breeder - Stress Considerations in Fuel Rod Design. K. M. Horst; March 28, 1960.

GEAP-3486 Fast Oxide Breeder Project - Fuel Fabrication.
Part I - Plutonium-Uranium Dioxide Preparation and Pelletized Fuel Fabrication, J. M. Cleveland, W. C. Cavanaugh;
Part II - Fabrication of Plutonium-Uranium Dioxide Specimens by Swaging. M. E. Snyder, W. C. Cowden; August 15, 1960.

GEAP-3487 Fast Oxide Breeder - Preliminary Sintering Studies of Plutonium-Uranium Dioxide Pellets. J. M. Cleveland, W. C. Cavanaugh; August 15, 1960.

GEAP-3646 Calculation of Doppler Coefficient and Other Safety Parameters for a Large Fast Oxide Reactor. P. Greebler, B. A. Hutchins, J. R. Sueoka; March 9, 1961.

GEAP-3721 Core Design Study for a 500 MWe Fast Oxide Reactor. K. M. Horst, B. A. Hutchins, F. J. Leitz, B. Wolfe; December 28, 1961.

GEAP-3824 Fabrication Cost Estimate for UO_2 and Mixed PuO_2 Fuel. G. D. Collins; January 24, 1962

GEAP-3833 The Post-Irradiation Examination of a PuO_2-UO_2 Fast Reactor Fuel. J. M. Gerhart; November 1961.

GEAP-3856 Experimental Fast Oxide Reactor. K. P. Cohen, M. J. McNelly, B. Wolfe; November 27, 1961.

GEAP-3876 Plutonium Fuel Processing and Fabrication for Fast Ceramic Reactors. H. W. Alter, G. D. Collins, E. L. Zebroski; February 1, 1962.

GEAP-3880 Comparative Study of PuC-UC and PuO_2-UO_2 as Fast Reactor Fuel. Part I - Technical Considerations, K. M. Horst, B. A. Hutchins; February 15, 1962. Part II - Economic Considerations, G. D. Collins; November 15, 1962.

GEAP-3885 Experimental Fast Ceramic Reactor Design. Status Report as of October 31, 1961. Edited by K. M. Horst; April 24, 1962.

GEAP-3923 Resonance Integral Calculations for Evaluation of Doppler Coefficients - The RAPTURE Code, J. H. Ferziger, P. Greebler, M. D. Kelley, J. Walton; June 12, 1962.

GEAP-4028 A Fuel Reprocessing Plant for Fast Ceramic Reactors. H. W. Alter; February 1, 1962.

GEAP-4058 Analytical Studies of Transient Effects in Fast Reactor Fuels, R. B. Osborn and D. B. Sherer; August, 1962.

GEAP-4090 FORE - A Computational Program for the Analysis of Fast Reactor Excursions, P. Greebler, D. B. Sherer; October, 1962.

GEAP-4092 Doppler Calculations for Large Fast Ceramic Reactors, Effects of Improved Methods and Recent Cross-Section Information, P. Greebler, E. Goldman; December, 1962.

GEAP-4130 Experimental Studies of Transient Effects in Fast Reactor Fuels, Series I, UO_2 Irradiations, J. H. Field; November 15, 1962.

GEAP-4226 Conceptual Design of a 565 MW(e) Fast Ceramic Reactor, A. Silvester; April, 1963.

GEAP-4271 Measurement of Oxygen-to-Metal Ratio in Solid Solutions of UO_2 and PuO_2, W. L. Lyon; May 31, 1963.

SECTION II

SUMMARY

2.1 Task B - Vented Fuel Development

Sodium logging tests were completed on three mixed oxide fuel specimens: an undefected control, a specimen fabricated with a central void containing sodium and having no defect for sodium escape, and a defected specimen subjected to 100 thermal cycles. Measurable cladding deformation occurred only with the last of these specimens. Maximum increase in clad diameter was but 8 mils (3 percent) even in this case and evidently resulted from a ratcheting mechanism due to the repeated cycling. Evidence of some sodium-fuel reaction was also noted in the two specimens containing sodium.

In oxide fuel-sodium compatibility tests conducted at 1050 - 1200 F, negligible reaction was observed with stoichiometric UO_2 of density greater than 89 percent of theoretical, pellet disintegration was observed with hyperstoichiometric UO_2. Slight grain boundary attack was observed on irradiated mixed oxide fuel.

Fabrication of fuel specimens for fission product plugging and fission product release to sodium experiments is nearly completed. Final capsule designs depend upon assignment of test reactor location.

2.2 Task C - Fuel Testing in TREAT

The second 0.25-inch diameter mixed oxide fuel specimen underwent transient irradiation which raised the peak fuel temperature to an estimated 6500 F. Slight bowing of the fuel specmen was observed and a possible slight increase in pin diameter. Internal examination revealed extensive central void formation and axial movement of molten fuel.

The first two specimens, planned for transient testing of previously irradiated mixed oxide fuel were successfully irradiated together for four weeks in GETR. One specimen will be used as the control for comparison with the second which is scheduled for TREAT irradiation.

Pre-irradiation has been initiated of three additional specimens scheduled for higher burnup exposure (ca. 50,000 MWD/T, requiring about 50 weeks in GETR) prior to transient testing in TREAT.

2.3 Task E - Fuel Performance Evaluation

Pre-operational testing of the central temperature measurement capsule has included cycling of the pressure transducers, compatibility studies of tungsten and rhenium thermocouple materials with mixed oxide fuel, thermal cycling of the end plug penetration and investigation of assembly and welding procedures.

Feasibility of evaporating thin layers of oxide on mixed oxide pellets has been demonstrated as a means for depositing Pu-242 traces for planned plutonium migration studies. Ultrasonic drilling of 0.014 inch diameter cores has been successfully tested as a fuel sampling procedure, using UO_2 as a stand-in for mixed oxide fuel.

Control of mixed oxide fuel pellet stoichiometry (over the O/M range 1.97 - 2.00) during sintering has been shown to be achievable by adjusting the water vapor content of the 6 percent H_2 - 94 percent He sintering furnace gas.

2.4 Task F - Fast Flux Irradiation of Fuel

Drawings received from ANL of a test subassembly to accommodate nonreinsertable, "standardized" capsule for EBR-II test irradiation are being reviewed. Based on the new design and consistent with the currently expected startup of EBR-II, a revised irradiation plan and schedule have been proposed.

2.5 Task G - Reactor Dynamics and Design

Parametric studies have been made on several different core compositions and geometries for a large FCR (~1000 MWe) with diameter to height ratios of 2, 3, and 6. The use of a small volume fraction of moderating material appears beneficial, significantly reducing the maximum reactivity increment due to partial loss of sodium while appreciably increasing the Doppler coefficient.

Evaluation of the Pu-239 Doppler effect was made using the multilevel method with results in close agreement with those previously obtained using the single level method. Initial calculations indicate that the overlap of the U-238 and Pu-239 resonances (an effect recently noted by Codd and Collins) greatly reduces the positive Pu-239 contributions to the Doppler effect.

SECTION III

TASK B - VENTED FUEL DEVELOPMENT

3.1 Sodium Logging

Sodium logging studies were completed during the quarter and a first draft of a topical report prepared. It is felt that the two series of capsule tests performed to-date have illustrated that sodium logging phenomena should not be a limiting criterion for rating fast reactor fuel operating or test conditions.

3.1.1 Series I - UO_2 Fuel

Summation of this previously reported work on six capsules containing UO_2 fuel specimens continued in conjunction with the preparation of a topical report.

3.1.2 Series II - Mixed PuO_2 - UO_2 Fuel

The second series of sodium logging capsules was designed to investigate the sodium logging characteristics of mixed oxide fuels under "worst case" conditions, in view of the encouraging results from Series I. The salient operating characteristics selected are shown in Figure 3-1.

The nondefected control specimen (B-II-A) was irradiated last quarter; however, a resume of the irradiation is included for reference during subsequent discussion of post-irradiation evaluation. Specimens B-II-B and B-II-C were irradiated, and all three specimens were examined this quarter.

3.1.2.1 Specimen B-II-A

Specimen B-II-A, the nondefected control specimen, was irradiated during peak flux conditions of GETR cycle 41. The capsule operated at a linear power generation rate of 25 ± 2 kw/ft with an average clad surface temperature of 1168 F. The rod power, previously reported as 26 ± 2 kw/ft, has been revised to 25 ± 2 kw/ft based on a re-examination of the calorimetric data. The calculated value of $\int_{t_o}^{t_c} k d\theta$ for this fuel rod was 93 w/cm, assuming a gap conductance of 2000 Btu/hr-ft^2-°F.

Post-irradiation examination of Specimen B-II-A revealed no detectable changes in clad diameter or length.

A. Fuel Rod Number — B-II-A

Fuel Rod Power Level — 25 kw/ft or 820 $^{w}/_{cm}$

Number of Power Cycles — 8

Total time In-Pile — 250 min.

Fuel Rod Burnup — 57 $\frac{MWD}{T\,(U,\ Pu)}$

Average Clad Surface Temperature — 1165°F

(Reference Capsule)

B. Fuel Rod Number — B-II-B

Fuel Rod Power Level * — 25 kw/ft or 820 $^{w}/_{cm}$

Number of Power Cycles — 4

Total Time In-Pile — 72 min.

Fuel Rod Burnup — 18 $\frac{MWD}{T\,(U,\ Pu)}$

Average Clad Surface Temperature — 1263°F

(Pre-Cored Pellet-Core, 54 mils diameter, filled with Na)

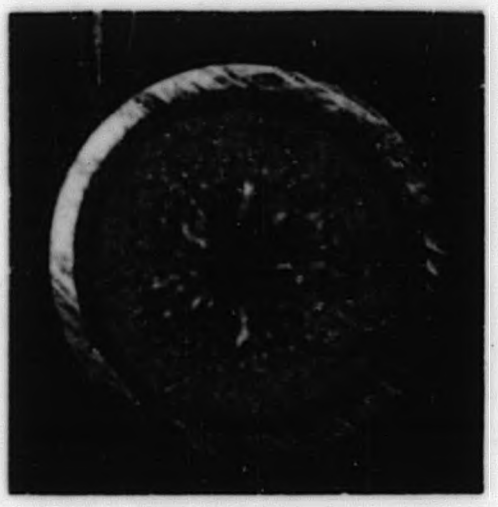

* Peak power level of 30 $\frac{kw}{ft}$ for approximately 10 seconds during initial startup.

C. Fuel Rod Number — B-II-C

Fuel Rod Power Level — 25 kw/ft or 820 $^{w}/_{cm}$

Number of Power Cycles — 100

Total Time In-Pile — 145 min.

Fuel Rod Burnup — 34 $\frac{MWD}{T\,(U,\ Pu)}$

Average Clad Surface Temperature — 1265°F

(Defected clad designed to open 5 mil hole in clad at center of fuel length at ~1100°F)

Figure 3-1. Photomacrographs of Series II Sodium Logging Fuel Cross Sections
Enrichment 20 $^{w}/_{o}$ PuO_2 - 80 $^{w}/_{o}$ UO_2

Metallurgical examination was accomplished in the new alpha enclosure facilities recently completed for low exposure, alpha contaminated work.

The fuel was sectioned and metallographic examination completed. The fuel microstructure, shown as Figure 3-2, exhibited a typical central void along with equiaxed grains in the outer areas of the fuel. No evidence of melting was detected.

An intriguing observation is that there is no evidence of lenticular pore sweeping as typically denoted by the characteristic large columnar grain formation. However, large grains with a distinct preferred growth direction are noted in the fuel which evidently were formed by a solid state mechanism other than pore migration.

A unique microstructure was noted at approximately two-thirds of the fuel radius from the center. Spherical shaped pores with a tail extending behind the pore exist in the structure. These pores and their distribution across the diameter are shown in Figures 3-3 and 3-4. In all cases the direction of pore migration was toward the fuel center. Many of these pores show arrest points in the tail structure, which suggests the arrest point for pore motion with each in-pile thermal cycle. The maximum rate of pore migration noted was 0.4 μ/minute based on maximum tail length and total irradiation time.

Moving spherical pores have not been reported in any of the UO_2 or PuO_2 fuel development literature. It is not known if this pore shape is primarily associated with mixed oxide fuel or is characteristic of short-time irradiations at high rod power.

The spherical pores are postulated to be porosity caught in the process of migrating to the fuel center to form a central void. The preferred location of the pores, shown in Figure 3-2, must be related to the thermal gradient which existed in the fuel. As the pores progress toward the fuel center their migration rate increases substantially. Thus, the observed pores are only those with low migration rates.

Presence of a second phase in the cooler portion of the fuel also can be noted in Figure 3-2.

3.1.2.2 Specimen B-II-B

Specimen B-II-B was designed to investigate a hypothetical "worst case" in which sodium had seeped into the center void without filling the pellet-to-clad gap, and the defect had become plugged subsequent to logging, thereby preventing sodium escape. To simulate this condition, the fuel pellets were core-drilled and the 0.054 inch diameter center hole filled with solid sodium. The "as-fabricated" fuel-clad gap was minimized by sizing precisely the inside diameter of the cladding, then selecting fuel pellel diameter to give 0.002 ± 0.001 inch gaps. The condition of minimum gap axially and radially was intended to represent the normally

observed case (FCR Phase 1) in which irradiated fuel pellets have expanded radially and closed the pellet-to-clad gap. Thus, peak central fuel temperatures were expected upon rapid insertion of this specimen into the flux, and the fuel volume at substantiallv lower temperature available for movement of sodium from the central void was minimized. The relative volumes in the completed specimen are tabulated in Table III-1.

TABLE III-1

SPECIMEN B-II-B VOLUME BREAKDOWN

	Percent of Total Volume	
	As Fabricated(1)	Operating(1)
Center hole (sodium filled)	4.6	4.5
Fuel	66.5	66.3
Void in fuel	4.0	4.0
UO_2 insulator pellets	20.5	20.1
Void in insulator pellets	2.6	2.6
Gap and end void	1.8	2.5
Total	100	100

(1) As-fabricated and operating temperatures of cladding assumed as 70 F and 1250°F, respectively; of fuel, 70 F and 2160 F (average).

The irradiation of capsule B-II-B occurred during peak flux conditions of GETR cycle 43. On the initial insertion into the GETR Trail Cable Facility, the sodium temperature exceeded the pre-determined safe value of 1300 F and the capsule was withdrawn. Two more somewhat-slower insertions resulted in similar excessive temperatures. A fourth slow insertion resulted in the design sodium temperature and the irradiation proceeded for one hour. Calorimetric data indicate a linear rod power of 25 ± 1 kw/ft. During the early operating history, which resulted in 125 percent of the design power, the capsule evidently was held against the wall of the Trail Cable Facility in a high flux region. Subsequent operation evidently heated the components, causing the capsule to reposition itself into a lower flux within the facility.

Examination of the fuel specimen showed no change in clad diameter or length.

The sodium temperatures during the initial insertion indicate that specimen linear power rate was 30 kw/ft or 25 percent overpower and the insertion time was ~ 1½ seconds. The estimated time at power for this initial insertion was 8 - 10 seconds. Although severe conditions were experience during each cycle of this irradiation, the first insertion represents

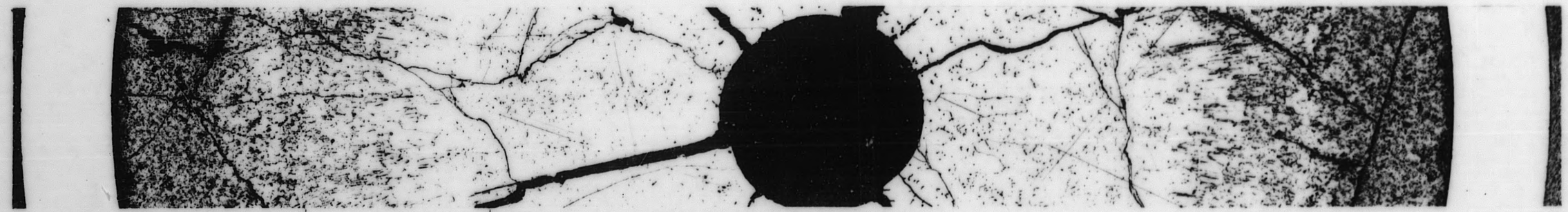

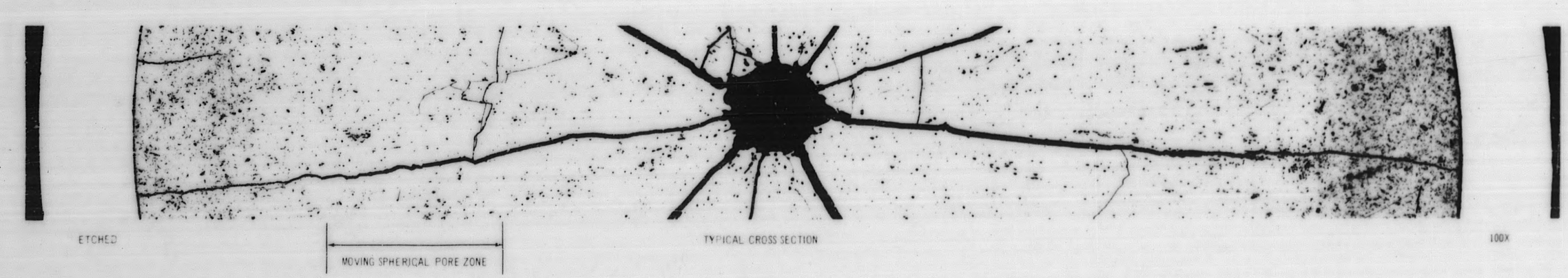

REDUCED TO 58% FOR REPRODUCTION

Figure 3-2. Photomicrographs of Two Fuel Cross Sections from Capsule B-II-A

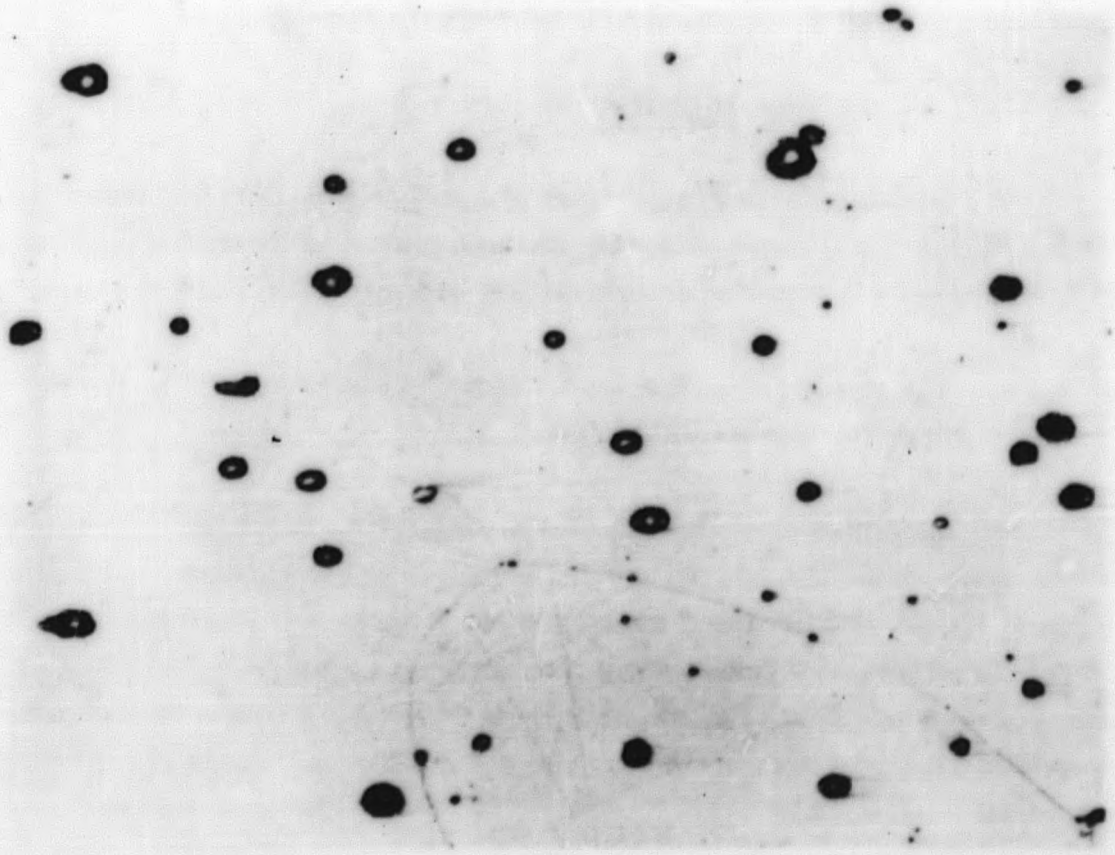

Figure 3-3. Spherical Pores in B-II-A

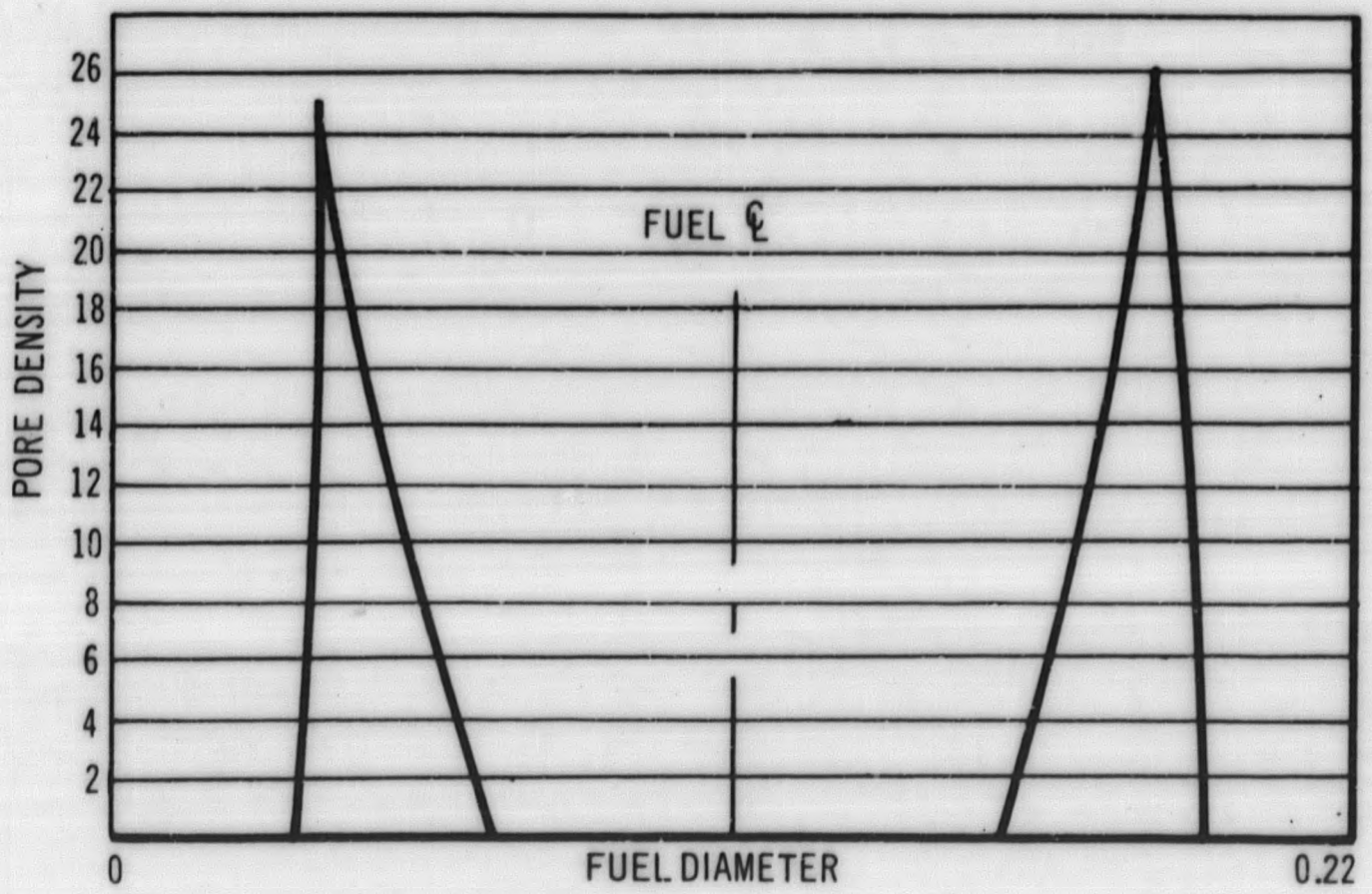

Figure 3-4. Moving Pore Density as a Function of Fuel Diameter in a Quarter Radian Section

the worst case because sodium redistribution into the fuel-clad gap probably occurred during this first cycle. Since the first cycle lasted only about ten seconds, a computerized transient heat flow analysis (TIGER V) was made, which established that the central fuel temperature actually reached essentially steady-state conditions equivalent to 30 kw/ft within this time. The results of the TIGER V analysis are shown in Figure 3-5.

Metallurgical examination of specimen B-II-B has revealed the microstructures shown in Figure 3-6. Since this specimen operated at maximum power levels near 30 kw/ft, much of the fuel microstructure formation probably occurred at this power.

The microstructure shows some evidence of melting as indicated by a porosity-free zone near the center of the fuel.

Specimen B-II-B also shows three structural boundaries (rings) around the fuel. The two outer rings are not defined by any significant changes in grain size or porosity. A comparison of the as-polished and as-etched structures in Figure 3-5 indicates that the outer ring was severely attacked by the etchant, resulting in complete removal of the fuel. The reacted zone corresponds to a region which evidently was "set-up" by the presence of sodium or possibly a sodium-fuel reaction product. The second ring probably represents the limit of sodium entry into the fuel (after redistribution from the center) during the cooler operating periods, i.e., at 25 kw/ft.

Movement of fuel into the pre-cored central hole can also be observed in Figure 3-6. The presence of what appears to be melted surfaces indicates that some radial molten fuel movement could have occurred, but gross slumping did not occur.

Evidence that very large moving pores were also caught in the B-II-B microstructure is shown in Figure 3-6.

3.1.2.3 Specimen B-II-C

Specimen B-II-C was designed to demonstrate the combined effects of sodium logging and repeated power cycling on FCR fuel. The cladding of this test specimen had a 0.005 inch defect similar to the UO_2 tests; however, in this case the defect was plugged with silver solder to permit alpha contamination control during fabrication in existing facilities.

This capsule was designed for operation for one hour at power to melt the silver solder plug, then for 100 power cycles from 3-to-24 kw/ft in less than 3 seconds, 30 seconds at 24 kw/ft, a rapid drop to 3 kw/ft, then 90 seconds at the low power, etc. The capsule was irradiated during GETR cycle 43 and operated as designed, except the peak power was 25 ± 1 kw/ft rather than 24.

Examination of the B-II-C fuel specimen revealed cladding expansion had occurred. The maximum diametrical expansion of eight mils occurred at the midpoint of the specimen. An expansion of two mils occurred 90 degrees from the maximum diameter. The total expansion along the length of the specimen is shown in Figure 3-7. This amount of expansion is not considered catastrophic, as regards progressive fuel failure, because fuel rod spacing is 100 mils in the reference design of the Fast Ceramic Reactor fuel assembly.

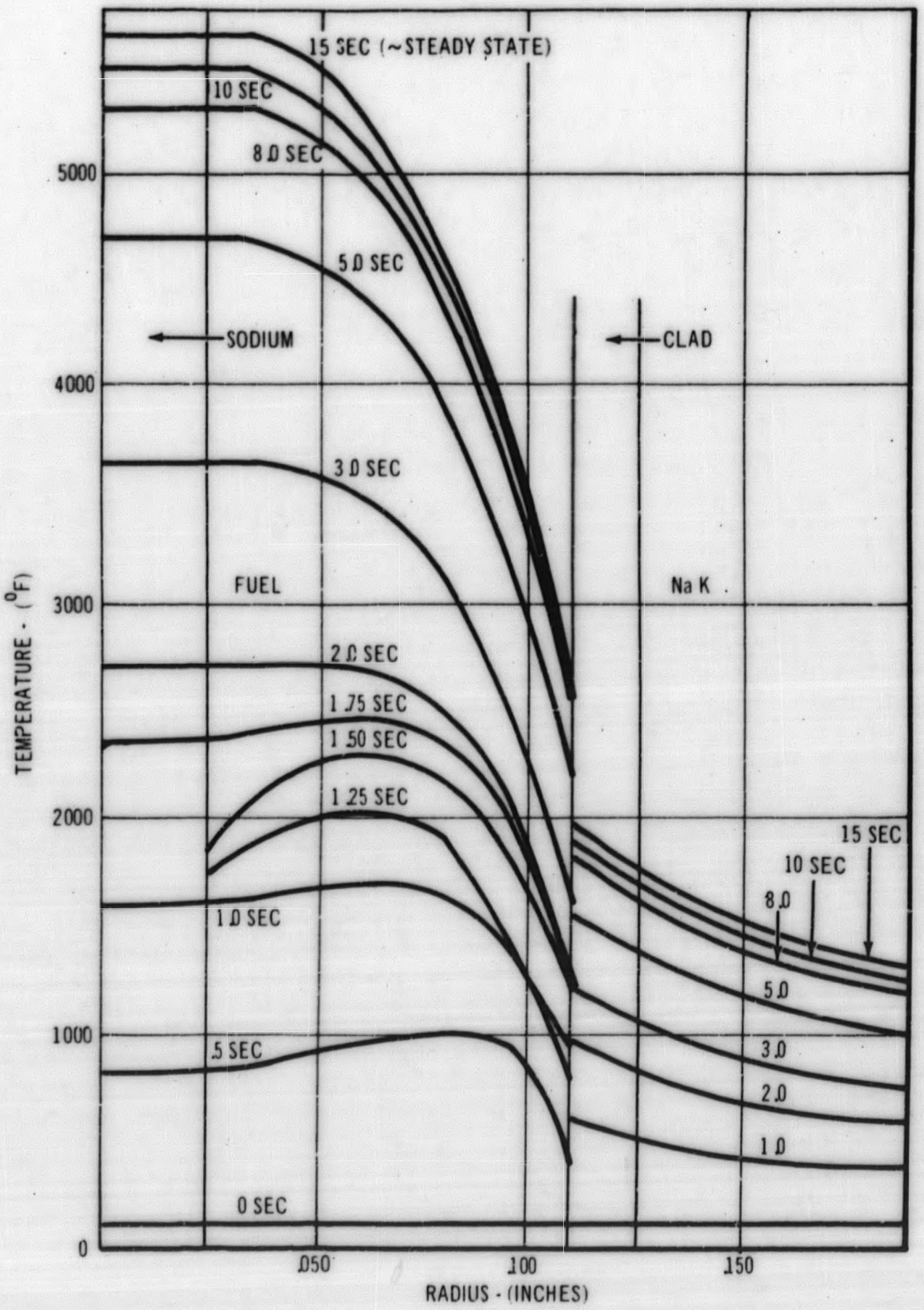

Figure 3-5. Calculated Temperature Profiles for the First Insertion of B-II-B

A metallographic examination was performed to determine whether the observed effect was caused by strain cycling and whether the strain was caused by sodium vapor pressure or fuel-clad interaction. The fuel microstructure is shown in Figure 3-8. The microstructure exhibits extremely large equiaxed grains with no center void. The large grains have resulted in a grossly cracked structure in the course of thermal cycling. The fuel pieces have participated in a radial ratcheting mechanism which has closed the fuel-clad gap and evidently damaged the clad.

The observations of large equiaxed grains and no central void suggest that sodium entered the fuel specimen a short time after the specimen reached full power. The entry of sodium into the fuel-clad gap reduced fuel center temperature and, possibly, quenched a structure typical of very short irradiation at high power. According to this hypothesis, the central fuel microstructure is one of large equiaxed grains prior to lenticular pore sweeping and central void formation.

Evidence of sodium-fuel interaction can also be observed in Figure 3-8. Note the gross presence of a second phase which is possibly a reaction product of Na, O, U, and Pu as evidenced by preferential etching of the material in the outer ring of fuel.

3.2 Sodium-Fuel Compatibility

Sodium-fuel compatibility has been investigated in both static and dynamic sodium tests using UO_2 fuel, and static sodium tests on irradiated, as well as unirradiated, mixed-oxide fuel. Tests have been performed at 1050 F to evaluate the effect on compatibility of O/U ratio, density, and time. Additional tests at higher temperatures are planned.

3.2.1 Static Na-Stoichiometric UO_2

UO_2 tests in static sodium capsules under isothermal conditions have continued to evaluate the effect on compatibility of density and time.

Low density (~82 percent TD) stoichiometric pellets have been reported previously as decomposing in contact with 1000 F sodium. Also, scouting tests indicated high density sintered UO_2 was not affected by 1050 F sodium.

A series of sealed capsules containing sintered UO_2 pellets with variable density were held in a furnance at 1050 F. The capsules were removed at intervals beginning after 6 hours and terminating after 840 hours.

The results of these tests have indicated that stoichiometric UO_2 pellets with density above 89 percent of theoretical density are not attacked significantly. The data are given in Table III-2. No difference was noted between centerless ground pellets and as-sintered pellets. In tests lasting more than 100 hours, a slight discoloration was noted on the UO_2 pellet surfaces. X-ray diffraction studies failed to show the presence of a second phase.

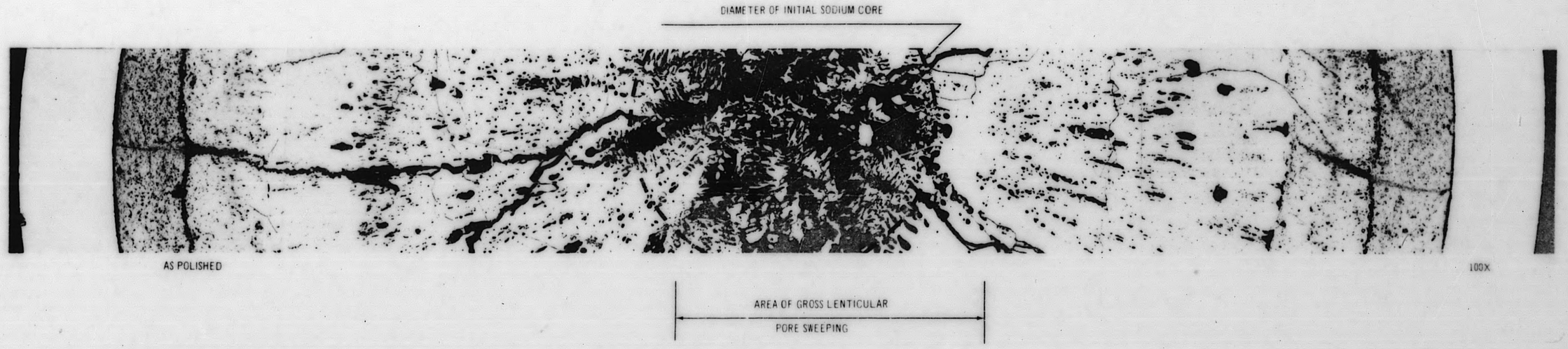

REDUCED TO 58% FOR REPRODUCTION

Figure 3-6. Photomicrographs of Fuel Cross Section from Capsule B-II-B

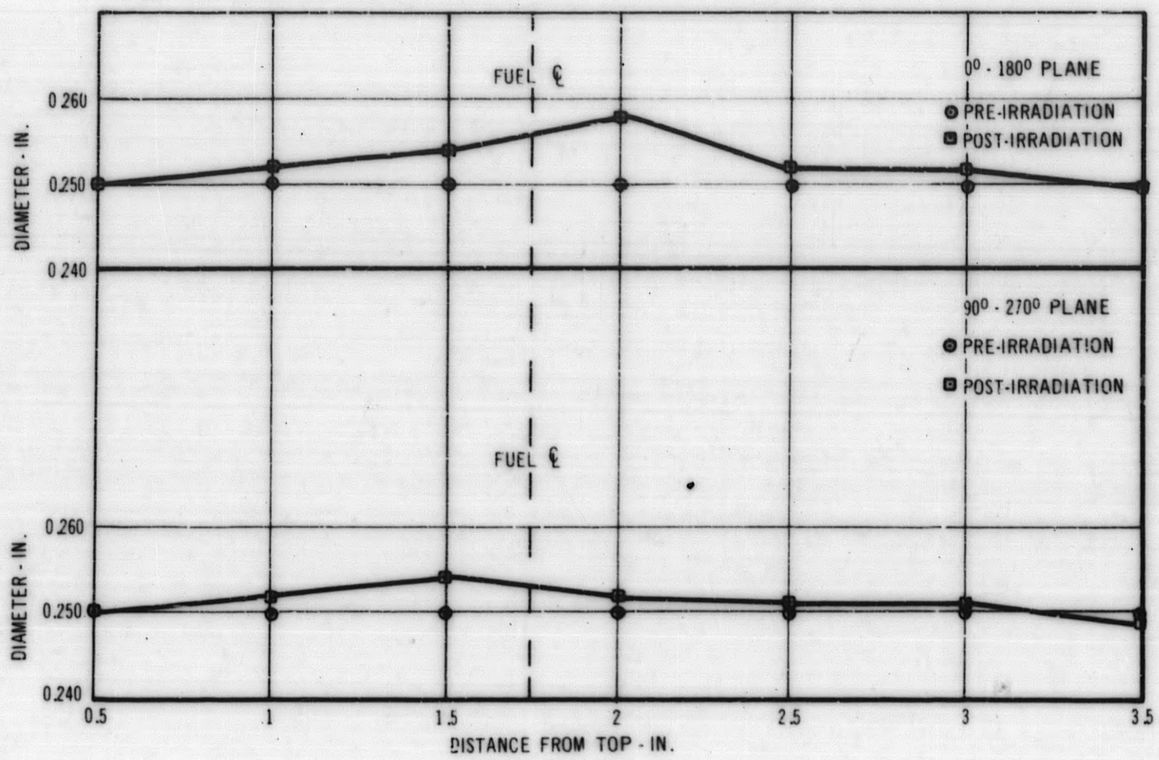

Figure 3-7. Pre- and Post-Irradiation Measurements - Capsule B-II-C

TABLE III-2

RESULTS OF STATIC Na-UO_2 TESTS AT 1050 F

Pellet	Density (% of Theoretical)	Exposure Time (hrs)	O/U Ratio	Pellet Change (%)	Remarks
B-1	96.6	0	2.00 ± 0.01	+0.6	Pellet intact
B-2	96.6	6	2.00 ± 0.01	-1.9	Pellet intact
B-3	95.5	51	2.00 ± 0.01	-2.5	Pellet intact
B-4	95.2	96	2.00 ± 0.01	-1.0	Pellet intact
B-5	94.2	168	2.00 ± 0.01	-1.6	Pellet intact
C-1	96.8	168	2.00 ± 0.01	-0.6	Pellet intact
C-2	86.5	168	2.00 ± 0.01	-0.1	Pellet intact
C-3	95.8	168	2.00 ± 0.01	nil (0.1)	Pellet intact
C-4*	96.4	168	2.00 ± 0.01	nil	Pellet intact
C-5*	96.2	168	2.00 ± 0.01	nil	Pellet intact
C-6*	96.3	168	2.00 ± 0.01	nil	Pellet intact
C-7	91.8	168	2.00 ± 0.01	+0.2	Pellet intact
C-8	91.4	168	2.00 ± 0.01	-1.9	Pellet intact
C-9	88.8	168	2.00 ± 0.01	nil	Pellet intact
C-10	88.9	168	2.00 ± 0.01	-0.8	Pellet intact
C-11	96.6	168	2.00 ± 0.01	nil	Pellet intact
C-12*	96.5	168	2.00 ± 0.01	nil	Pellet intact
C-13	96.4	336	2.00 ± 0.01	nil	Pellet intact
C-14*	96.4	336	2.00 ± 0.01	+0.1	Pellet intact
C-15	96.4	504	2.00 ± 0.01	-0.3	Pellet intact
C-16*	97.0	504	2.00 ± 0.01	nil	Pellet intact
C-17*	96.3	672	2.00 ± 0.01	+0.1	Pellet intact
C-18	96.5	672	2.00 ± 0.01	+0.5	Pellet intact
C-19	96.7	840	2.00 ± 0.01	+0.5	Pellet intact
C-20*	96.2	840	2.00 ± 0.01	+1.00	Pellet intact
S-10	97.4	168 hrs	2.19	--	Pellet disintegrated
S-27	92.5	168 hrs	2.10	--	Pellet disintegrated
S-11	97.0	1 hr	2.19	--	Pellet disintegrated
S-28	92.5	1 hr	2.10	--	Pellet disintegrated
S-12	96.3	5 min	2.19	~50	Partial attack
S-30	93.0	5 min	2.10	-1.0	Slight discoloration
S-14	96.6	1 min	2.19	-1.2	Pellet intact

All pellets weighed approximately 1.5 gms and were tested in 1 cc of sodium.

*Centerless ground

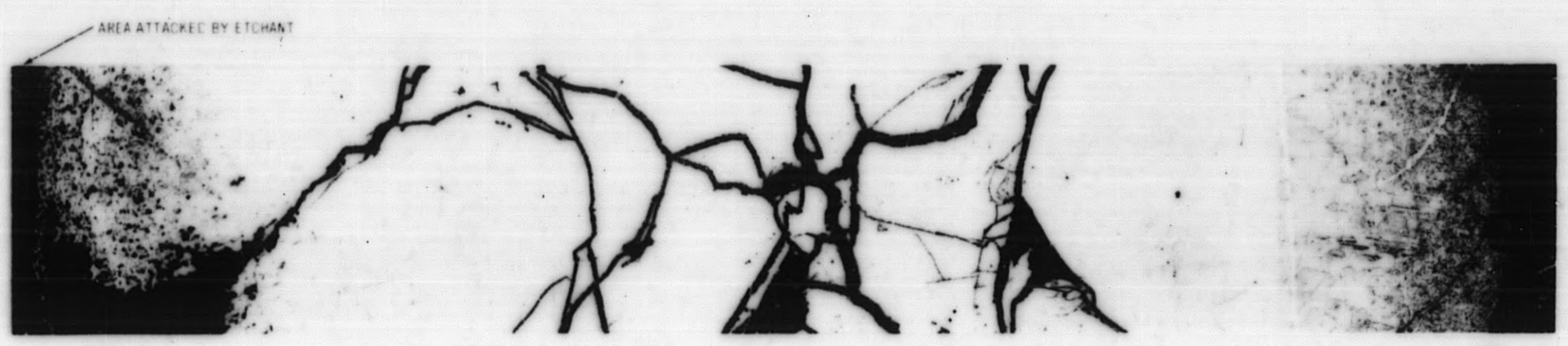

REDUCED TO 58% FOR REPRODUCTION

Figure 3-8. Photomicrographs of Fuel Cross Section from Capsule B-II-C

3.2.2 Static Na - Hyperstoicniometric UO_2

3.2.2.1 Fuel Production

Hyperstoichiometric UO_2 pellets have been prepared by steam sintering using argon as a pre-sinter and cooling atmosphere so as to retain excess oxygen.

Pellets with an average O/U ratio of 2.102 ± 0.002 and a density of 93 percent TD were prepared by sintering in steam at 1400 C for 30 minutes. X-ray diffraction studies showed a major phase with a lattice parameter of 5.466 Å ($UO_{2.06}$) and a trace of U_4O_9.

Pellets with an O/U ratio of 2.190 ± 0.008 and a density of 96.5 percent TD were prepared by steam sintering for two hours at 1400 C. X-ray diffraction analysis showed both U_4O_9 and $UO_{2.09}$ (lattice parameter = 5.464 A). According to the UO_2 phase diagram [1] the single phase UO_{2+X} is formed at elevated temperature during steam sintering. On cooling, some excess oxygen precipitates as U_4O_9, resulting in the two-phase structure of U_4O_9 and UO_{2+X}.

The variation of O/U ratio within the pellet was examined on one hyperstoichiometric pellet. The results are illustrated in Figure 3-9. The data points were determined by successive dissolutions of the pellet surface using deoxygenated anhydrous phosphoric acid followed by coulometric O/U measurement on each fraction. The depth of penetration was determined by uranium material balance.

3.2.2.2 Na Tests

A series of static sodium tests to evaluate the effect on compatibility of O/U ratio and time were completed. These tests show that sodium and hyperstoichiometric UO_2 react at 1050 F with the end result of complete pellet disintegration in short time periods. Data are given in Table III-2. Comparison of the 5-minute tests shows that the relative reaction rate of 2.19 O/U ratio pellets is greater than that of the 2.10 O/U ratio pellets. An effort to identify the reaction product is in progress.

3.2.3 Dynamic Sodium - UO_2 Tests

A series of tests of UO_2 and UO_{2+X} pellets have been completed in the FCR sodium loop at 1050 F. The results of the tests are summarized in Table III-3.

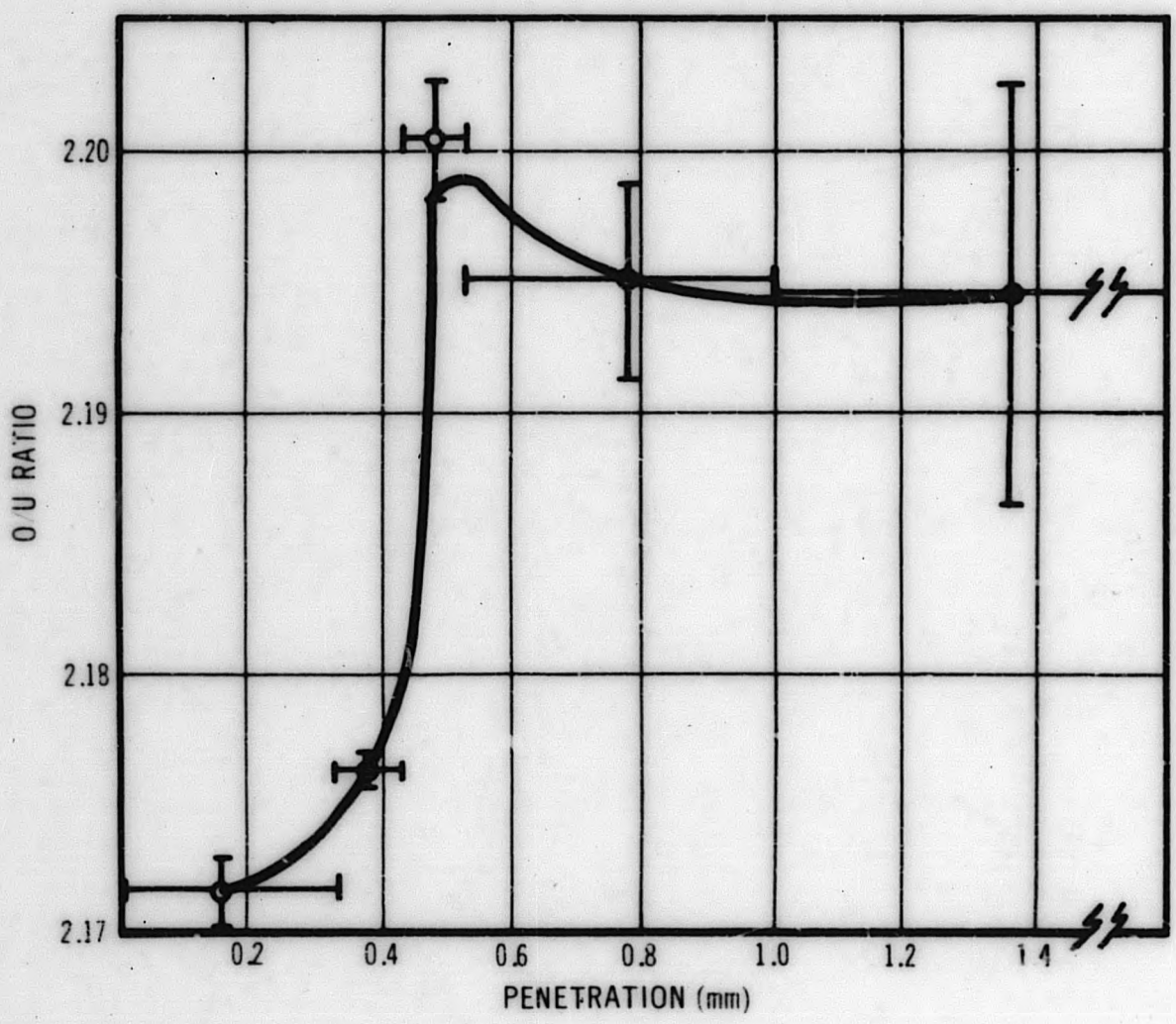

Figure 3-9. O/U Profile of Hyperstoichiometric UO_2 Pellets

TABLE III-3

UO_2 PELLET - SODIUM COMPATIBILITY TESTS AT 1050°F*

(flow rate = 16.5 ft/sec)

Test	Test Period (hrs)	O/U Ratio	Density gm/c.c.	Initial Weight (gm)	Final Weight (gm)	Remarks
2	118	2.01	10.77	38.61**	38.64	Slight surface reaction
2	118	2.01	10.33	39.05**	39.07	Slight surface reaction
3	263	2.01	10.44	38.99**	39.00	Slight surface reaction
5	27	2.10	10.14	1.60***	-	decomposed
4	168	2.18	10.49	1.80***	-	decomposed
4	168	2.18	10.61	1.72***	-	decomposed

*Oxide content of sodium varied from 10 to 190 ppm.

**Annular pellet 1 inch OD · 0.6 inch ID · 0.5 inch long.

***Cylindrical pellet 0.22 inch OD · 0.25 inch long

These tests show results identical to those predicted by capsule tests on similar UO_2 pellets (see Section 3.2.2).

3.2.4 Static Na-Irradiated PuO_2 - UO_2 (Phase I)

Four experiments were conducted in the Radioactive Materials Laboratory (RML) to determine the compatibility of high burnup 20 $^{w}/_{o}$ PuO_2-80 $^{w}/_{o}$ UO_2 fuel with liquid sodium at coolant temperatures expected in the FCR. The specimens selected for these tests had experienced burnups between 30,000 and 70,000 $^{MWD}/_{T}$ (U, Pu) at power levels between 6 and 19 kw/ft. Both swaged and pelleted fuel sections were used for this study. The irradiated specimens had been stored in air for approximately two years prior to their use in these sodium compatibility tests.

Table III-4 lists the irradiation parameters and dimensions of the test samples (ca. one-inch long) prior to sodium exposure. The fuel sections were tested with the fuel and surrounding clad as shown in Figure 3-10. Both ends of the fuel section were open to permit the liquid sodium to flow through the existing central void, thereby offering maximum surface area for any possible sodium-fuel reaction. The fuel sections were loaded into the test capsules and sealed under an argon atmosphere. In all cases the fuel sections were completely submersed in sodium during the tests.

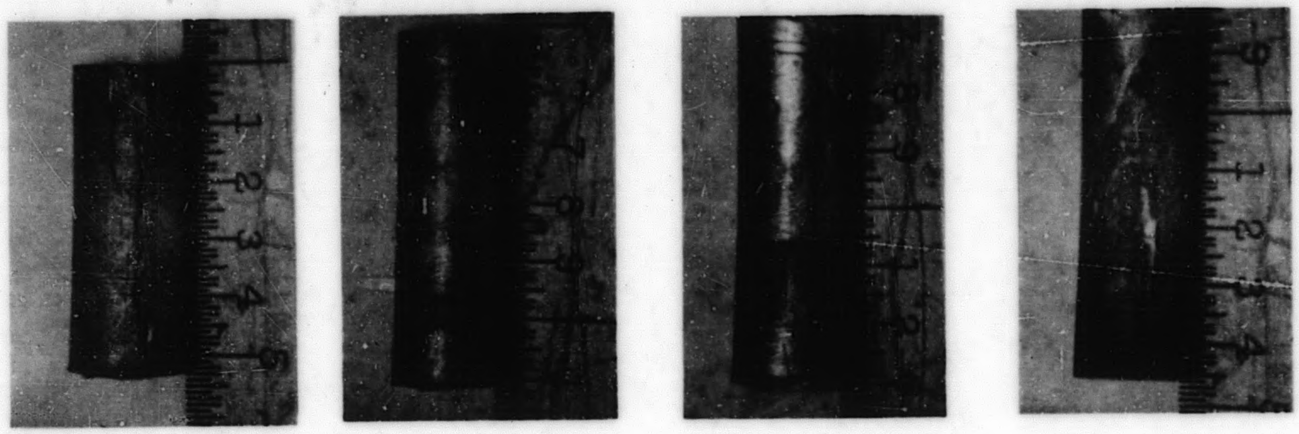

8703-01	8706-01	8705-01	8704-01
VII-1-S	IX-2-P	VI-3-P	VI-4-S

Figure 3-10. Post-Sodium Exposure Appearance of Test Specimens

TABLE III-4

SPECIMEN SIZE AND IRRADIATION HISTORY OF TEST SAMPLES

Sample	Burnup MWD T(U, Pu)	Burnup f/cc 20 x10	Avg. kw ft	Pre-irradiated Density (% TD)	Clad OD	Clad ID	Clad Type	Clad R. A. of Swaged Specimens	Cold Radial Gap (mils)
VII-1-S[b]	70,300	12.7	19.0	75	0.190	0.150	304 SS	42%	0
IX-2-P	38,300	8.8	17.0	94.8	0.189	0.156	347 SS	0	3
VI-3-P	34,900	7.8	8.15	92.3	0.189	0.156	347 SS	0	3
VI-4-S	30,900	5.6	5.8	75	0.190	0.150	304 SS	42%	0

a. Fissions per cm^3 based on pre-irradiated fuel density and a value of 200 mev/fission.

b. S and P designate swaged and pelleted fuel, respectively.

The welded test capsules were heated in a resistance furnace at 1200 F (650 C) for a total of 20 hours. The samples were cycled to test temperature a total of three times during the 20-hour period.

No gross sodium-fuel reaction was noted in any of the fuel sections studied; however, slight attack in the grain boundary areas, particularly in the fuel center section, was noted. Upon etching of metallographic specimens (with 10 percent HNO_3 - 20 percent H_2O_2 aqueous solution) severe grain boundary attack and subsequent loss of part of the specimen occurred. Figure 3-11 shows the pre- and post-sodium microstructure of specimen VII-1-5 which was typical of the other three samples.

There appears to be no gross reaction between static sodium and irradiated 20 w/o PuO_2 - 80 w/o UO_2 at temperatures of 1200 F. Evidence of slight grain boundary attack was noted in all microstructures in the as-polished and as-etched samples. A possible explanation of the phenomenon is as follows:

Previous investigators have reported that UO_2 can dissociate at elevated temperatures.[2] When 20 w/o PuO_2 - 80 w/o UO_2 is heated to a high temperature, the solid solution may also lose a certain fraction of its oxygen. Some of this excess oxygen will enter the grain boundary which acts as a sink for impurities or excess oxygen. Thus the oxygen-to-metal ratio in the grain boundary would be significantly higher than in the matrix grain. Any excess oxygen in the mixed oxide lattice in the grain boundary should react with sodium in much the same manner as hyperstoichiometric UO_2 does. (See Section 3.2.2.) This theory is somewhat substantiated by the in-pile test B-I-E of the sodium logging experiment in which a distinct grain boundary reaction was again noted with sodium in the fuel.[3]

3.3 Fission Product Plugging

Detailed design of an irradiation capsule, intended to proof-test the vented-through-blanket design of vented fuel elements, was discontinued during the report period pending resolution of test reactor siting. The experiment was tentatively assigned to MTR/ETR on 5/20/63 by the USAEC. Detailed descriptions of the experiment and experimental flux requirement were prepared and forwarded to Phillips Petroleum Company to check the feasibility of completing the work in MTR/ETR.

During the period, design and fabrication of the test fuel rod for the first capsule (B-III-A) were continued. The final design is shown in Figure 3-12. The design features a long fuel rod equipped with a fission gas reservoir. The length of the assembly is determined by the maximum capabilities of existing plutonium laboratory facilities. A temporary welding enclosure for completion of this work has been designed and fabrication started at the end of the period.

The fuel rod for capsule B-III-A is comprised of 22 inches of mixed PuO_2 - UO_2 fuel, and 19 inches of natural UO_2 blanket, with a fission gas reservoir situated above the blanket. To conserve length, a dual-diameter reservoir has been designed so that the internal volume is about equal to the fuel volume as in the reference design. The fuel cladding is 0.25-inch diameter 0.015-inch wall, 347 stainless steel. Thermocouples are situated along the length of the fuel and blanket and in the reservoir for measurement and control of fuel performance.

A pressure sensor is situated on the top of the reservoir to detect the buildup of fission gases. A null balance pressure system is planned utilizing the stainless steel diaphragm shown on the drawing. Design of the out-of-pile portion of the pressure monitor is continuing. Thermocouples placed in the reservoir will be used to detect temperature changes so that pressure-temperature corrections to the data are possible.

Fabrication of 20 $^{w}/_{o}$ PuO_2 - 80 $^{w}/_{o}$ UO_2 sintered pellets is nearing completion. These pellets will constitute 95 ± 1.5 percent TD fuel with 2.00 ± 0.005 O/M ratio. Tight dimension control is expected to result in pellet-to-clad gap control between 0.001 to 0.003 inch. Fabrication of the natural UO_2 blanket fuel is also near completion.

3.4 Fission Product Release

The irradiation of the first three capsules, designed to study fission product release from FCR fuels, was tentatively assigned to MTR/ETR on 5/3/63, by the USAEC pending feasibility and cost comparisons of MTR/ETR and GETR. An MTR capsule concept and detailed descriptions of the experiment were prepared and forwarded to Phillips Petroleum Company.

Fuel specimens for three capsules, B-IV-A, B-IV-B, and B-IV-C, were fabricated during this quarter. These specimens were described in the Sixth Quarterly Report, GEAP-4214.

PRE-SODIUM MICROSTRUCTURE (AS POLISHED)

100X

POST-SODIUM MICROSTRUCTURE (ETCHED)

100X

REDUCED TO 58% FOR REPRODUCTION

Figure 3-11. Comparison of Pre- and Post-Sodium Microstructures of Specimen VII-I-S

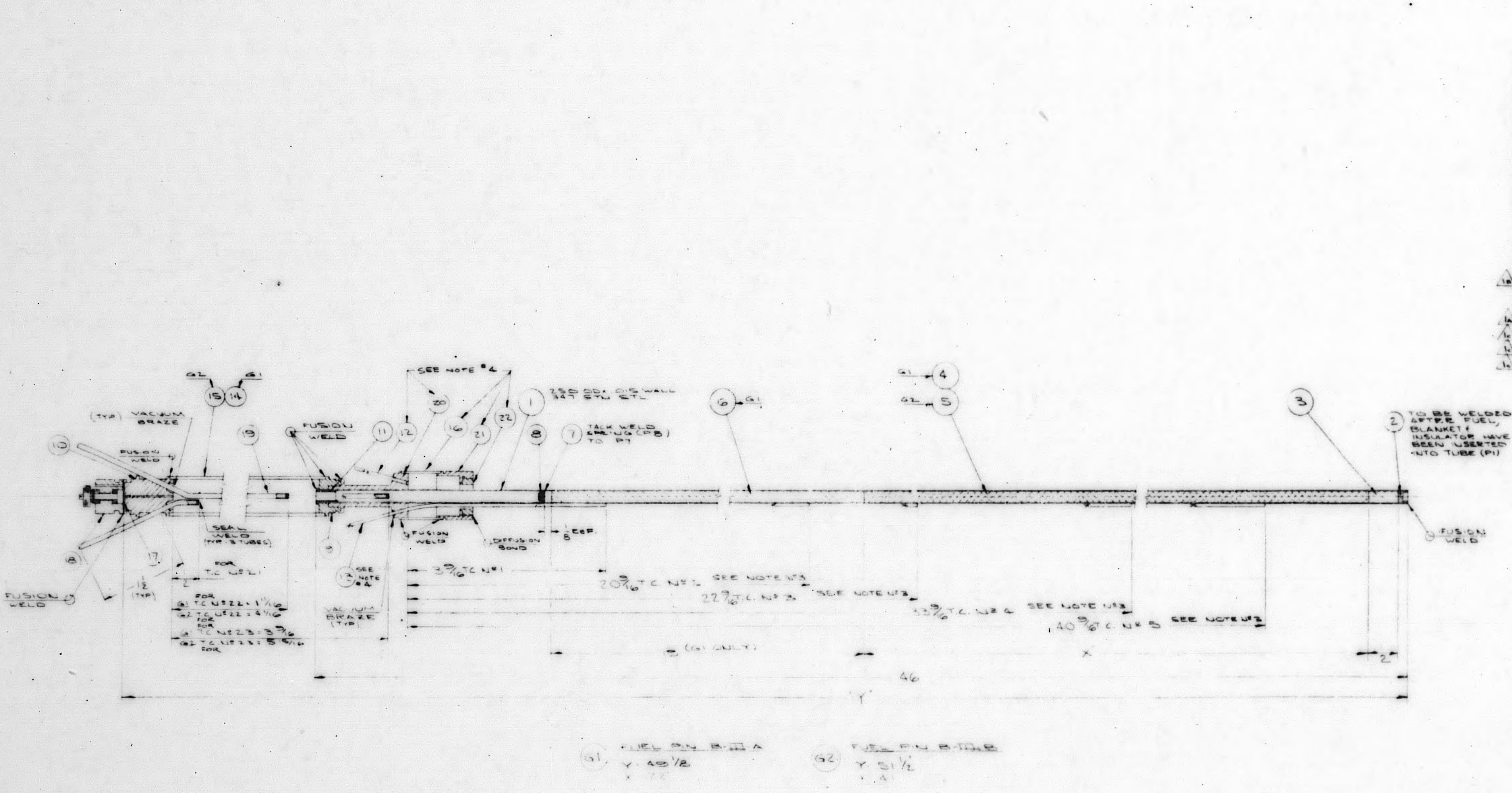

Figure 3-12. Fuel Pins B-III-A and B-III-B (Based on GE Drawing 144F689)

SECTION IV

TASK C - TRANSIENT TESTING OF FUEL

4.1 Series I Tests

Series I testing of 1.0-inch diameter, UO_2-fueled specimens has been completed and distribution of a topical report [4] has been made.

4.2 Series II Tests

A total of three transients have been run to date on two Series II specimens (0.25 inch OD stainless steel clad, mixed 20 $^{w}/_{o}$ PuO_2 - 80 $^{w}/_{o}$ UO_2). Estimated temperatures of ~6500 F have been achieved in the fuel region. One more test remains to be specified in this series.

4.2.1 Specimen II-A

This initial experiment of Series II was subjected to two TREAT transients producing estimated peak fuel temperatures of ~3000 and 4900 F. Initial sectioning of this pin was accomplished in the Plutonium Fabrication Laboratory as described in the preceding quarterly report.[3]

4.2.1.1 Post-Irradiation Examination

Following the initial sectioning operation, the specimen was transferred to the RML alpha enclosure for further disassembly and examination. The bottom half of the fueled section was impregnated with Hysol resin and a 3/4-inch metallographic sample prepared. The examined surface was located approximately 3-3/4 inches from the bottom weld. An attempt was made to remove the fuel pellets intact from the upper half of the fuel section by shaking and tapping the sample gently. Each of the fuel pellets appeared to be fractured radially, however, and were tightly lodged in the cladding. The UO_2 insulator pellets were removed from each end of the fuel stack and were apparently not damaged by the irradiation.

Metallographic examination of the fuel material was completed. Significant visual observations made during the examination were as follows:

a. An apparent porosity gradient was noted from the central region to the outer edge of the fuel pellet, indicating a severe temperature gradient near (~0.020 inch) the pellet surface. The appearance of the central 1/3 of the fuel diameter, however, indicated a more isothermal condition as predicted from computed temperature vs. time relationships.

b. A definite increase in grain size from the edge to the center of the pellet was also observed. The grains at the center were roughly twice the size of the grains at the outside surface, with the increase beginning at approximately one-fifth of the radial distance in from the edge, and remaining nearly uniform from this point to the center of the sample. This grain size distribution again confirmed the computed temperature profiles and indicated temperatures well in excess of the sintering temperature (~3000 F) were reached in the pellet central region.

c. The region of marked grain size increase also exhibited a double grain boundary type of structure which may be the impressions of old boundaries remaining as grain growth occurs. In each case the old and new boundaries follow the same pattern, exhibiting the appearance of a double image. This structure is believed to be due to the rapid transient quenching of the fuel and is another indication of the extreme thermal gradient present near the pellet surface.

d. Six major radial fractures and numerous microcracks were present in the fuel pellet in the examined plane. There were no circumferentially oriented fractures of significance in this specimen, as might be expected in fuel subjected to steady-state operating conditions.

It was concluded from these observations, plus a comparison with Series I results, that peak fuel temperatures in this specimen reached the melting point of the mixed oxide (~4900 F) in the second transient as computed. The absence of any evidence of once-molten material, however, suggests that the energy input fell short of supplying the full latent heat of fusion.

4.2.2 Specimen II-B

Since no clad distortion or other damage was found in the first test specimen, it was planned to continue to a more severe transient case in which a portion of the fuel reached a peak temperature in the liquid range (i.e., beyond the heat of fusion).

4.2.2.1 Calculations

Computer calculations made before the test indicated that a 200 MWsec clipped transient, on an initial period of 0.16 sec (~1.25 percent ΔK reactivity insertion) would result in an average fuel temperature peak of ~5600 F and a capsule equilibrium condition of 1100 F (starting at a pre-heat temperature of 800 F).

Calculations have shown that the fuel temperature in these small diameter (0.25 inch) pins is very much a function of the initial transient reactor period, due to the relatively short time constant involved. Thus it is found that at a point in time shortly after the

peak transient power is reached, the specimen begins to release its heat to the surrounding medium at a higher rate than the internal generation. At this point the fuel temperature reaches a maximum, and the remainder of the power pulse serves only to raise the equilibrium temperature.

4.2.2.2 Irradiation

On March 29, 1963, capsule II-B was subjected to a 204 MWsec transient, initiated on a 0.135-sec period with a 1.35 percent ΔK reactivity insertion. This pulse resulted in an equilibrium temperature rise of 311 ± 29 F indicating a total sample energy release of 70 ± 7 Btu. Attempts to simulate this transient with the TIGER V computer code have shown good correlation with the observed sodium and heat sink temperatures. It is estimated that the peak fuel temperature reached some 6500 ± 500 F with the volumetric average fuel temperature peaking at ~6000 ± 500 F (see Figure 4-1). Thus, the estimated fuel temperatures reached were somewhat higher than the expected values, due to a slightly shorter initial period than requested. This variation was still within the target range of the test, and fuel temperatures remained below the estimated region of substantial vapor pressures.

By comparison, the maximum transient in Series I (specimen I-D), resulted in an estimated peak fuel temperature of ~7300 ± 400 F[4] which gave rise to a measured pressure pulse of 800 psig. Thus, the difference in peak temperatures in the two tests (may be as great as 1700 F) could account for a very substantial difference in vapor pressures generated in the fuel.

4.2.2.3 Post-irradiation Examination

Disassembly of the capsule was accomplished in the RML and a sample of the NaK analyzed for plutonium. Negative results indicated that no cladding penetration occurred in the course of the transient.

Dimensional checks indicated a maximum bow in the fuel of 0.124 inch and possibly a slight increase in diameter (~0.001 inch) near the center of the fueled section. The major portion of the bowing centered at six inches from the bottom of the pin. A measurement was made to determine the force required to straighten the fuel pin and was found to be approximately eight pounds.

The sample energy release was again determined with nondestructive gamma radiation analysis using the photopeak for lanthanum-140 and barium-140. This method indicated a burnup of 0.021 ± 0.002 MWD/T which was equivalent to an energy release of 64 ± 6 Btu for sample II-B. This agreed within 10 percent of the value calculated from calorimetric measurements.

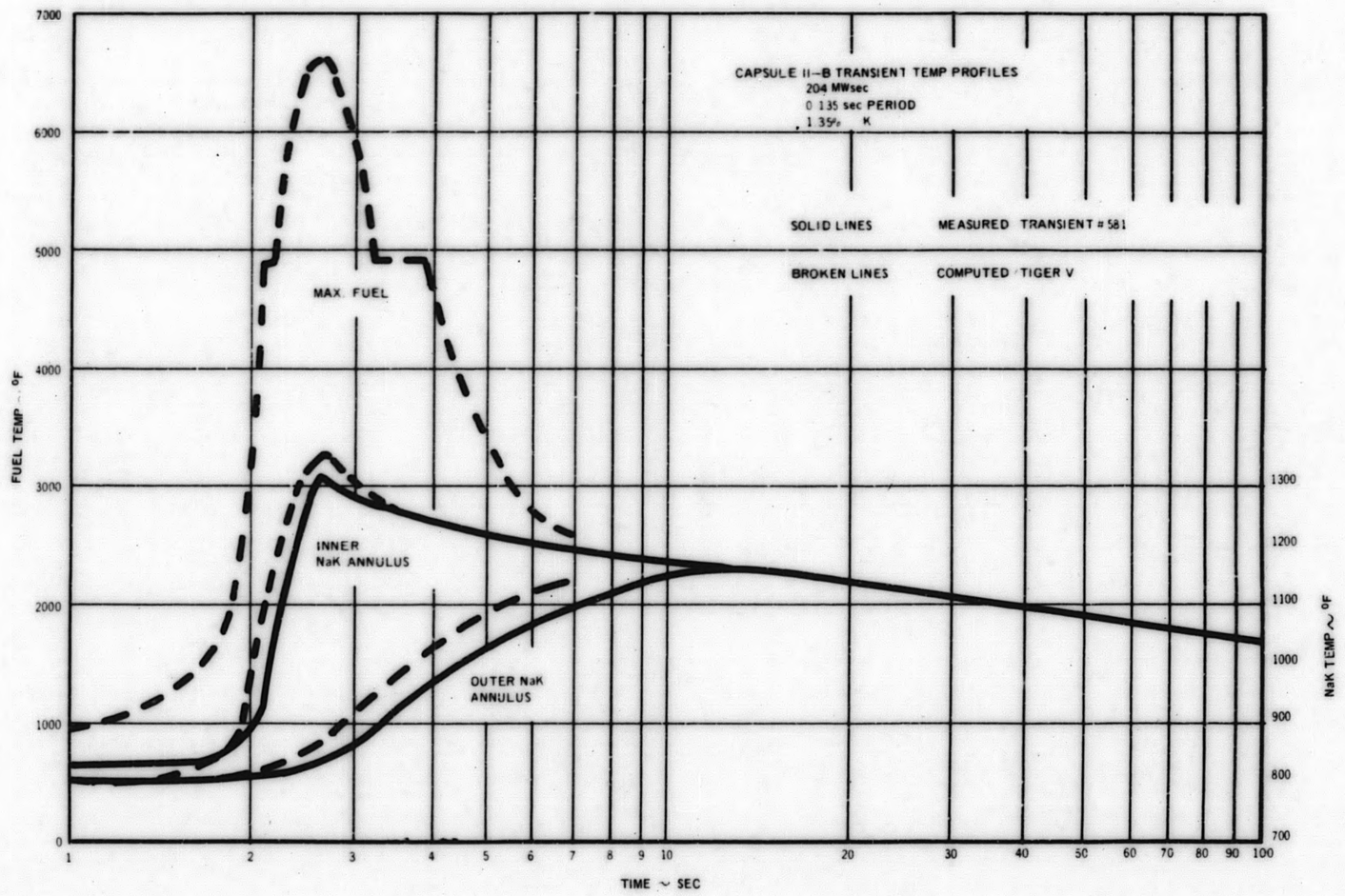

Figure 4-1. Capsule II-B Transient Temperature Profiles

An attempt to obtain a sample of gas within the pin to analyze for oxygen as an indication of dissociation of PuO_2 was unsuccessful due to mechanical difficulties.

Internal examination of the pin was initiated by making transverse sections at intervals throughout the fuel and lower insulator regions (see Figure 4-2). During the course of this sectioning, a central void was observed to extend down from the top of the fueled region a distance of some four inches. At the top of the fuel stack this void accounted for approximately 60 percent of the fuel cross-sectional area.

At the lower end of the fuel section, the pre-fabricated central hole in the UO_2 insulator pellet was filled with what appeared to be a solid plug of fuel material. This plug extended at least $\frac{1}{2}$-inch downward into the cored insulator pellet as indicated in the lower two sections illustrated in Figure 4-2.

Three metallographic specimens were prepared as indicated in Figure 4-3. Evidence of extensive central void formation and downward movement of molten fuel are evident in these polished sections. One longitudinal section illustrates the lower end of the fuel column where the mixed oxide has been quenched as it flowed into the cored insulator pellet. The upper longitudinal section contains a conical-shaped central void which was probably initiated as a result of downward fuel movement and then amplified by the volume change in going from the liquid to solid state $(-9.6\ \Delta V/V)$[5], in much the same manner as a shrinkage cavity is formed in a casting. This mechanism would support the contention that the central portion of the fuel rod was completely filled with molten fuel at peak power during the transient; this molten fuel core was contained by a ceramic shell of PuO_2 - UO_2.

The bridge-like structure noted in the upper section of Figure 4-3 is shown in the etched condition in Figure 4-4 at approximately 50X magnification. It seems likely from studies of this cross section, that the bridge was formed by the downward flow and subsequent solidification of molten fuel material into a previously formed central void. This is evidenced by the outline (of the previous central cavity) which became visible in the etching process. This outline is obviously a continuation of the central void at the lower end of the section which must have been formed early in the transient.

The upward movement of fuel noted in the Series I transients and the apparent downward flow of fuel as noted in Figure 4-3, indicate that considerable fuel movement must occur when a significant percentage of the fuel is heated to the melting point. Previous studies by Lyons[6] on high power UO_2 tests show that significant clad swelling occurs when fuel rods operate with a molten core without any room for fuel movement.

4.3 Series III Tests

The first two capsules in this series were irradiated for four weeks in GETR as planned during cycle number 42. Three more of these capsules are now under irradiation in GETR and are scheduled to attain burnups in the range of 50,000 MWD/T before TREAT irradiation. All specimens in this series are identical to those in Series II (0.25 inch OD stainless steel clad, mixed-oxide pellets), except that the PuO_2 - UO_2 ratio is slightly higher initially (28 percent PuO_2) to provide a representative composition after pre-irradiation.

4.3.1 Specimens III-A and III-B

Capsules III-A and III-B were irradiated for one cycle in the X-9 and X-10 GETR pool positions during cycle number 42. Temperature measurements during the cycle indicated sample power generation of 24.8 to 17.5 kw/ft for III-A and 20.9 to 14.5 kw/ft for III-B. In both cases the power peaked early in the cycle, as expected, and tapered off as control rods were withdrawn. GETR attained a total of 829.3 MWD for the cycle, of which 821.4 MWD were logged at full power.

Specimen III-A will be used as the control specimen to be examined before TREAT irradiation of III-B. It is expected that the internal appearance of III-A will give acceptable indication of the condition of III-B before TREAT irradiation.

Examination of III-A has progressed to disassembly of the capsule and removal of the fuel specimen. No significant change was noted in dimensions or profile and the outward appearance of the pin is essentially unchanged. An attempt will again be made to sample the gas within the pin prior to sectioning (the foreign material found in specimen II-B is not present in the hole leading to the diaphragm in III-A).

Re-encapsulation of specimen III-B for TREAT will proceed as soon as possible. Pressure transducers have been received and bench tests are being performed to develop installation procedures on pre-irradiated capsules. Present plans call for transient pressure instrumentation on all Series III specimens in TREAT.

4.3.2 Specimens III-C, III-D, and III-E

Capsules III-C, III-D, and III-E were irradiated in GETR pool positions Z-10, Z-12, and Z-13, respectively, during cycle number 44. Temperature measurements during this cycle indicated sample power generation rates of 25 to 19 kw/ft for all three specimens, with III-E running slightly higher (~5 percent) than the other two. GETR attained a total of 630.7 MWD for the cycle, of which 621.4 MWD were logged at full power.

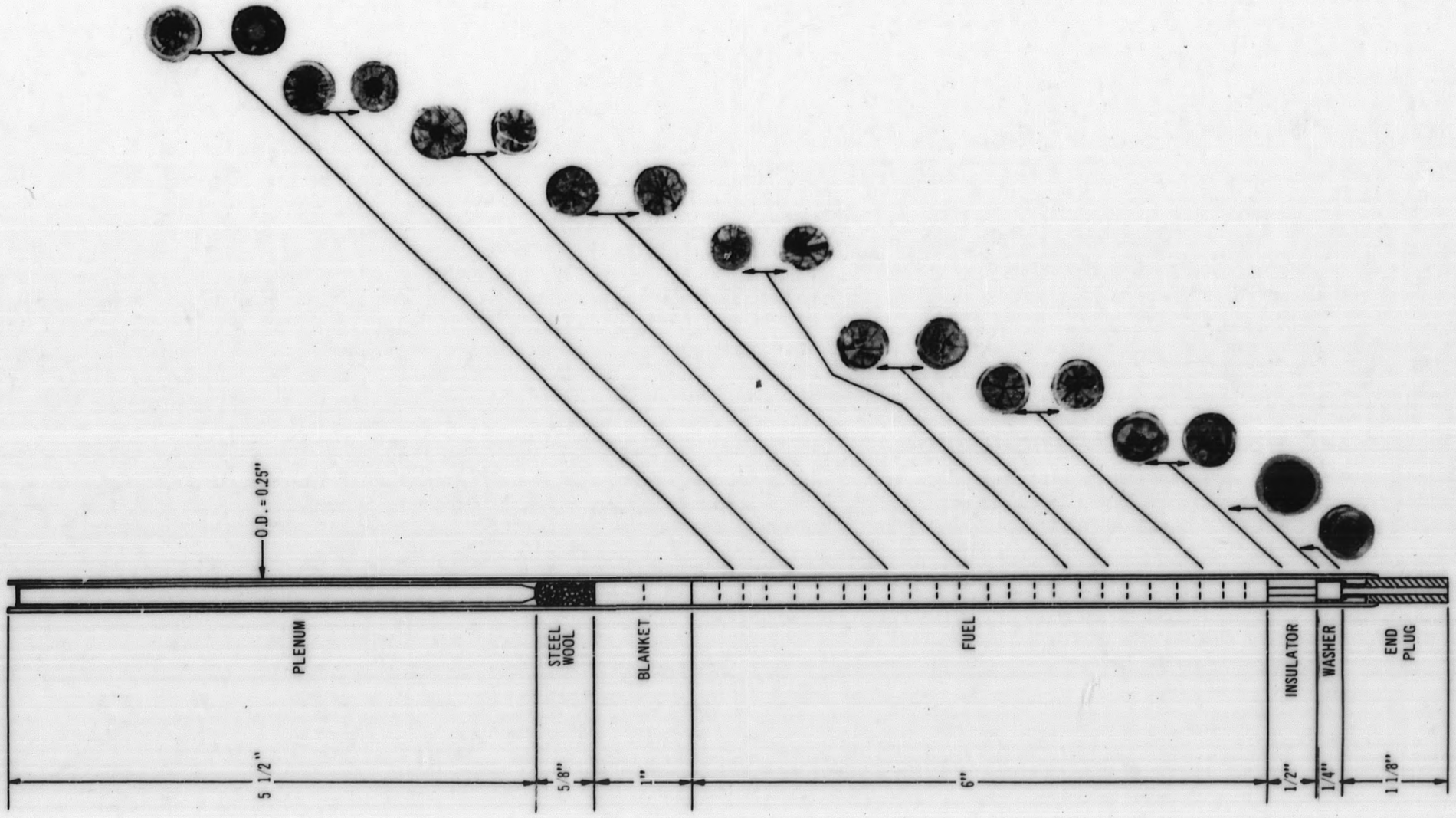

Figure 4-2. Transverse Sections of Specimen II-B, As-Cut Condition

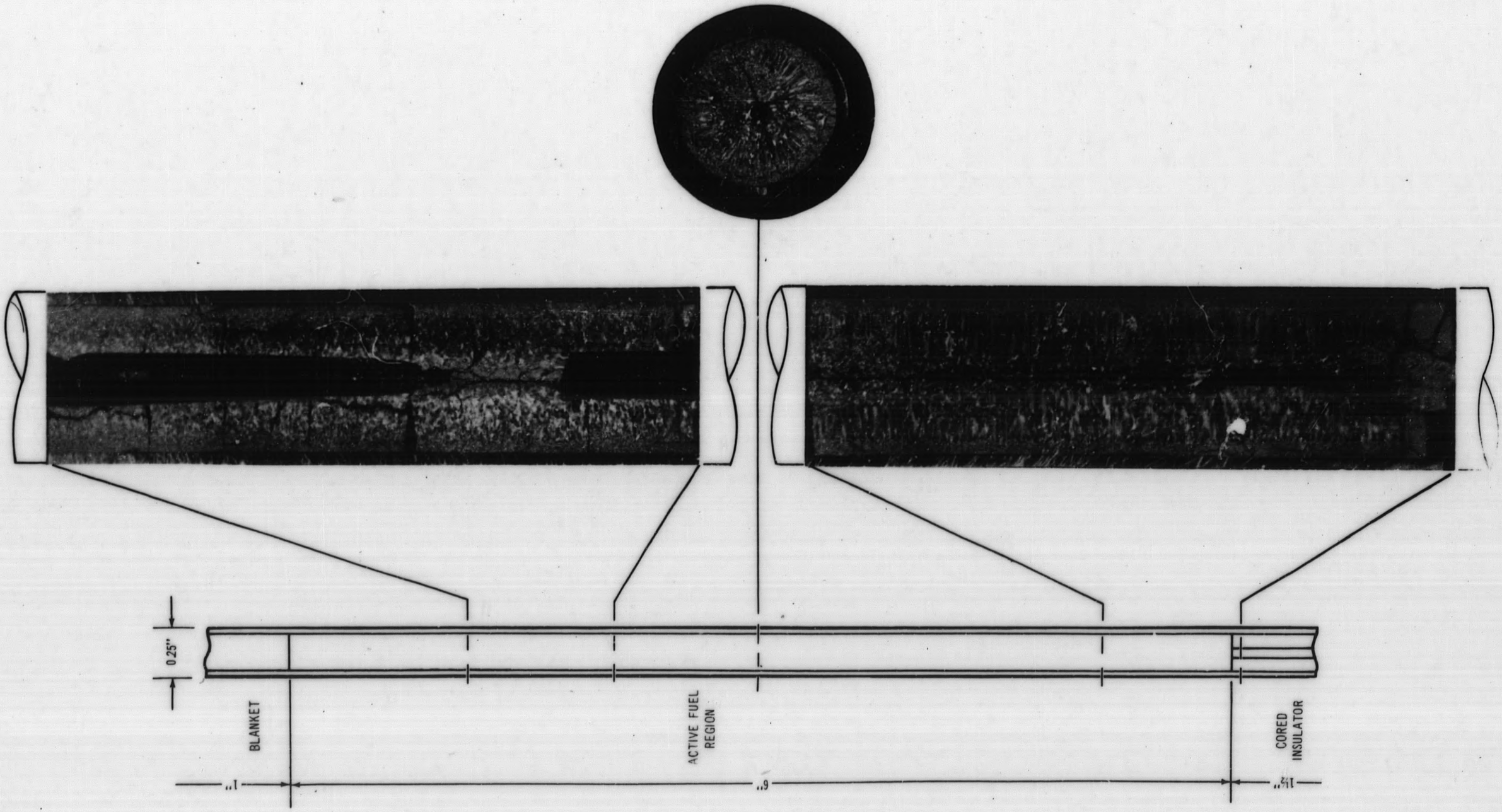

AS POLISHED PHOTO MACROGRAPHS OF SPECIMEN II-B

Figure 4-3. As-Polished Photomacrographs of Specimen II-B

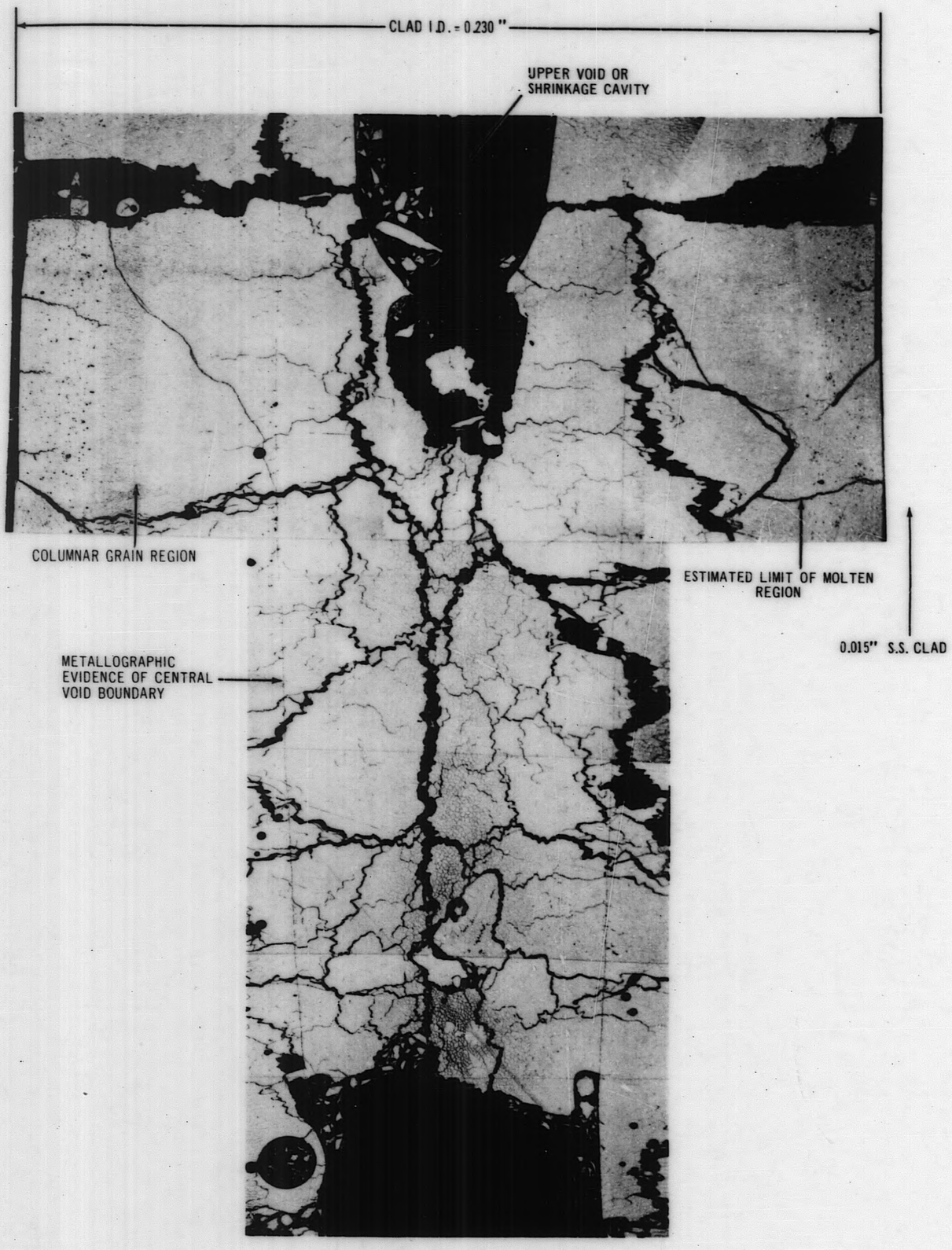

Figure 4-4. Photomicrograph of "Bridge-Like" Section from Specimen II-B

SECTION V

TASK E - FUEL PERFORMANCE EVALUATION

5.1 Central Temperature Measurement of Mixed Oxide

An irradiation capsule carrying two fuel pins equipped with gas thermometers and high temperature thermocouples has been designed. Fabrication was started in June.

Final Capsule Design

The fuel pin drawings and fabrication specifications have been signed off and issued. The capsule assembly drawings and fabrication specifications have been circulated for comments and will be signed off by mid-July. The data package and analysis for Safeguards approval is currently being prepared.

Figure 5-1 shows an exploded view of the final capsule and pin design.

Table V-1 summarizes the design parameters. Irradiation approval Form 21 has been submitted and approved; Form 22 has been submitted. Completion of the capsule and auxiliary systems is scheduled for September and irradiation is expected to begin in October.

A 52 inch long mockup, complete with thermocouple junctions and end plugs. is being prepared for a test of assembly and welding procedures in the Plutonium Laboratory. The welding box where this will be done has been completed including modification on the welding jig. This facility consists of a one-inch OD aluminum tube, approximately 52 inches long extending to the floor, which rotates at approximately 1 rpm in O-ring seals to permit welding of the end-plug.

Thermocouples

The 0.090 inch central temperature tungsten-rhenium thermocouple is scheduled for delivery at the end of July. Final iteration on the design (aimed at minimizing thermionic effects in the thermocouple) was sent to the vendor in June.

A test specimen of the fuel pin end-plug penetration by the tungsten-rhenium thermocouple and by the stainless steel capillary connection to the pressure transducer was fabricated, brazed, and tested by thermal cycling successively to 600 F and 1200 F. Helium leak tightness to the limit of detection (4×10^{-10} cc/sec) was maintained.

TABLE V-1

CAPSULE E1A SUMMARY DATA SHEET

I. Fuel Pins

		Pin 1	Pin 2
Fraction PuO_2		20 w/o	0 w/o
Fraction UO_2		80 w/o	100 w/o
UO_2 enrichment in $U^{235}O_2$		40%	70%
Stoichiometry, O/M ± 0.005		2.00	2.00
Fuel:	Shape	Sintered hollow pellets	
	outside diameter	0.220"	
	inside diameter	0.100" ± 0.002	
	sintered density	93.5% TD	
	active fuel length	3"	
Clad:	material	SS 347	
	outside diameter	0.250"	
	thickness	0.015"	
Cold diametral clearance		0.002 ± 0.001"	
Insulator pellets:		natural UO_2	

II. Capsule Design

Length	64"
Outside diameter	1-1/8"
Primary material of construction	Zircaloy II
Thermal bonding of capsule internals	NaK
Thermal dams	Zr-2 and Al annuli

III. Irradiation Conditions

Location	GETR pool
Cycle average thermal flux	$9 \cdot 10^{13}$ nvt
Beginning of cycle peak/cycle average flux	1.76
Vertical repositioning range of capsule during cycle	18"
	peak/min. = 2.7
Radial repositioning range during cycle	3-1/8"
	peak/min. = 5
Peak thermal flux setting; capsule mid-plane	$1.25 \cdot 10^{13}$ nv

TABLE V-1 (Continued)

IV. Thermal Conditions

(By axial positioning, the peak conditions of the all-urania Pin 2 will be kept equalized with the mixed oxide Pin 1.)

Peak hot spot power available at start of cycle

Fuel lineal power generation		30 kw/ft
Fuel surface-to-center $\int kd\theta$*		4400 Btu/hr-ft
Temperatures:	fuel center*	4400°F
	fuel outer surface	2200°F
	clad surface	1000°F
	capsule surface	210°F
	capsule cooling water	110°F
Heat Flux:	clad surface	$1.56 \cdot 10^6$ Btu/hr-ft^2
	capsule surface	$0.331 \cdot 10^6$ Btu/hr-ft^2

Capsule Cooling

Capsule heat removal	53,000 Btu/hr
Minimum water flow	12.8 gpm
Water temperature rise	4.1 F
Pressure drop	20 psi
Fuel burnup, 1 cycle	10,000 MWD/T

V. Instrumentation

Water calorimetry	4 thermocouples
Linear power	4 thermocouples
Fuel central temperature	Two W-26-Re thermocouples
	Two gas-bulb thermometers
Water flow (controllable)	D.P. Cell

*Based on UO_2 conductivity

Fuel Pin Fabrication

Pilot runs on the mixed oxide pellet fabrication have been made. Some difficulty had been experienced in obtaining full density of the all-urania 70 percent enriched pellets for pin E1A-2. Using an oxidation-reduction cycle temperature of 350 C, it was possible to obtain density to meet specification. Pellets pressed with a green density of 5.5 to 5.7 reached a fired density of 90-to-93 percent TD. Green densities of 5.7 to 6.0 resulted in fired densities of 93 -to-95 percent TD. The pellets were fired at 1700 C in wet hydrogen.

A preliminary run of fabrication of mixed oxide bushings (hollow pellets, 0.220 inch OD and 0.100 inch ID) was done by pressing with a cored die. This test (five pellets) yielded a slightly undersize ID which was enlarged by burr-drilling. The 70 percent enriched UO_2 pellets for pin E1A-2 were produced by drilling solid sintered pellets, with good yields. This procedure is also being adopted for the mixed oxide pellets, in preference to the cored die.

Fabrication

Parts for the fuel pin end-plug and pressure transducer assembly were started in June. An extra pressure transducer was fabricated and has been pressure-cycled to 1000 psi 4200 times in an endurance test.

Auxiliary Equipment

The pressure transducer readout system design is complete and fabrication is on schedule. Capsule header water supply system final drawings have been prepared and approved. Fabrication is scheduled for July.

Bids on capsule instrumentation have been received and orders will be placed in July. An eight-week delivery quote for the temperature reference junction block may require the borrowing of a similar component for startup tests.

Repositionable Capsule Equipment

A second iteration of drawings was prepared in June, but problems remain in attaining the desired reproducibility of positioning and of position indication. A new type of cable (ball-bearing-type) is being evaluated to obtain the required precision of horizontal movement.

Compatibility Studies - Mixed Oxide with Rhenium and Tungsten

Compatibility limits of tungsten and rhenium with 20 percent PuO_2 - UO_2 are of interest in determining thermocouple limitations. A small quantity of approximately stoichiometric mixed oxide (20 percent PuO_2) was sealed in a 1 inch length of 1/16 inch rhenium tubing by welding longer lengths of 1/16 inch rhenium rods into its ends. This tube was then resistance-heated in an argon atmosphere at 150 psig. The tube was subjected to the following heating schedule: 1-1/2 hour at 1800-1825 C; 6-1/4 hours at 2220-2250 C. At the end of the second

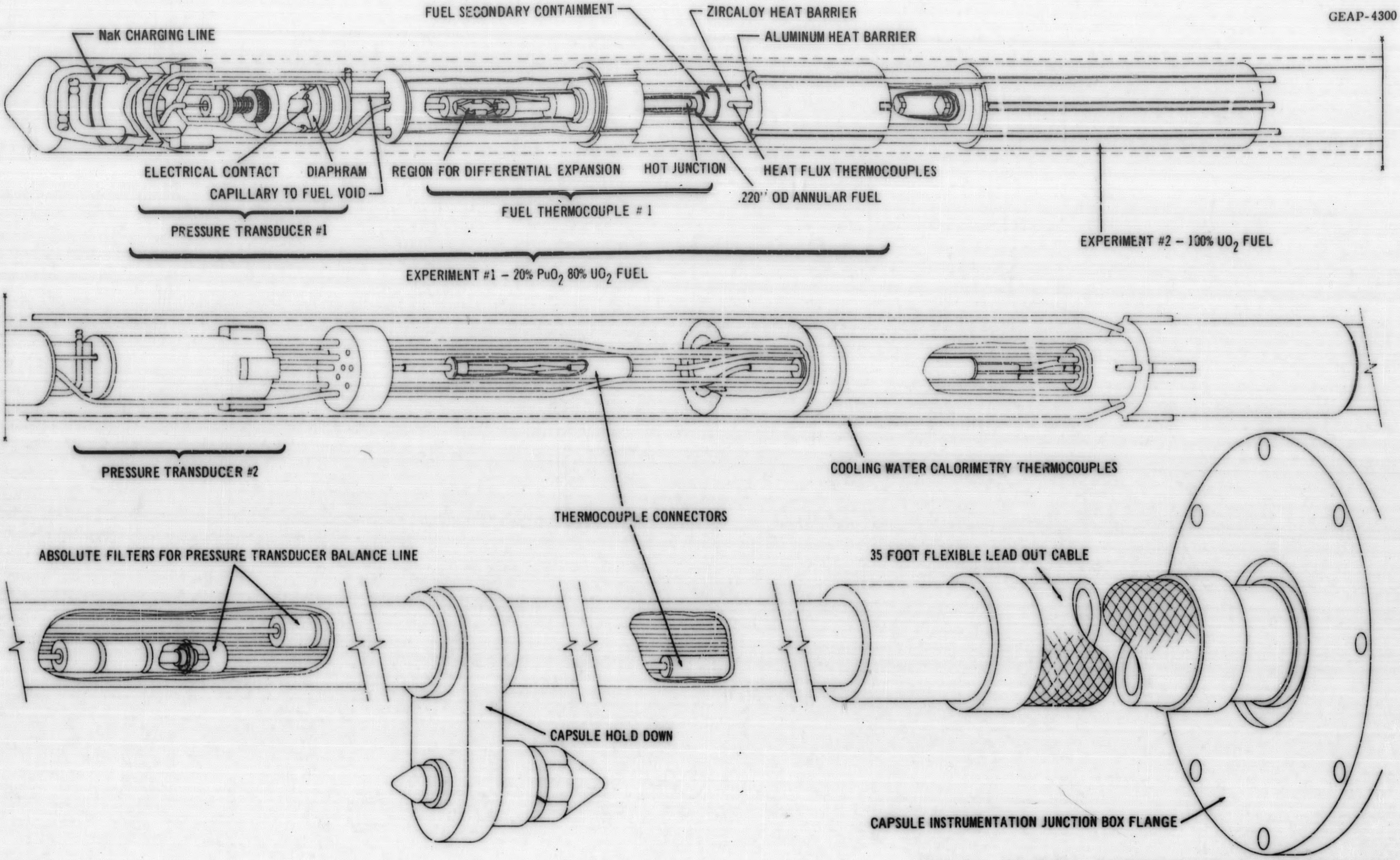

Figure 5-1. Capsule E1A - Fuel Temperature Measurement and Conductivity

heating period the tube developed a visible slight offset at the center, due either to reaction of the oxide with the metal or to a local "hot spot" resulting from loss of metal by evaporation (probably as the oxide due to trace impurities in the argon). The tube is being examined metallographically. This experiment will be extended to temperatures above the mixed oxide melting point and to oxides of varying stoichiometry.

Three attempts to prepare similar experiments with tungsten tubes have not been completed because of either porosity in the tubing or cracking at the welds.

5.2 High Burnup Irradiations

Irradiations of well-characterized oxide fuel samples of controlled stoichiometry are scheduled in capsules E2A and E2B. Capsule E2A uses 0.220 inch OD mixed oxide fuel and will operate at nominal FCR peak specific power (~128 watts/g of total uranium and plutonium, peak-to-average ratio of 2.0, and hot spot factor of 1.5). Capsule E2B uses 0.150 inch OD fuel which permits operation at approximately 1.8 times the nominal peak specific power, and correspondingly shortens the irradiation time to a given burnup target. The two sizes are believed to bracket the range of performance of economic interest to large oxide-fuelded fast reactors.

Each capsule contains two fuel pins of different stoichiometry: namely O/M ratios of 1.97 and 2.04. One of the irradiations under Task B (capsule B-III) will effectively complete the E2A series - with similar peak operating conditions and a stoichiometry of 2.00. (The effects of more extreme values of O/M on fuel properties are being explored in connection with plutonium migration, discussed in the next section.)

Final capsule designs have been completed. Figure 5-2 is typical of both E2A and E2B which differ mainly in the diameter of the fuel pins. Table V-2 gives the design parameters and peak operating conditions.

Fabrication of pins and capsules is scheduled to start in July and to be completed in September. Process development for preparation of the 1.97 and 2.04 O/M mixed oxide pins is covered in Section 5.5.

5.3 Plutonium Migration

Capsule E3A, containing a set of plutonium migration experiments, is planned to operate in-pile for one month at conditions both above and below the melting point of mixed-oxide fuel. Six pins of varying stoichiometry are placed end-to-end in a single 1-1/8 inch diameter capsule. Plutonium and uranium diffusion in solid, liquid, and vapor phases in the individual pins will be traced by plutonium-242 and uranium-233 isotopes deposited by vapor deposition techniques on selected pellet surfaces. Temperature profiles will be obtained from measurement of the central temperatures of two of the specimens using tungsten-26-rhenium thermocouples, and derived for

TABLE V-2

LONG BURNUP PIN CHARACTERISTICS

		Pin Designation			
	Tolerance	E2A-1	E2A-2	E2B-1	E2B-2
Location in Capsule		lower	upper	lower	upper
Fuel pellet:					
PuO_2 composition by weight	±0.5%	20%	20%	20%	20%
UO_2 composition by weight	±0.5%	80%	80%	80%	80%
UO_2 enrichment in U-235*	±0.5%	40%	40%	40%	40%
Length/Diameter ratio ≥		1	1	1	1
O/M Ratio	±0.015	2.040	1.970	2.040	1.970
Clad: SS type		347	347	347	347
ID (inches	±0.002	0.220	0.220	0.150	0.150
Pellet-clad diametral gap (inches)	±0.001	0.002	0.002	0.002	0.002
Fuel Length (inches)	±0.10	8.00	10.00	8.00	10.00
Axial gap, pellets-to-end plug (inches)	±0.020	0.080	0.080	0.080	0.080
Insulator Pellets:					
Length (inches	±0.020	0.250	0.250	0.250	0.250
Gap (inches)	±0.001	0.002	0.002	0.002	0.002
O/M Ratio	±0.005	2.00	2.00	2.00	2.00
Power Output, Peak**					
kw/ft	±5%	28	28	22.5	22.5
kw/kg (U+Pu)	-	405	405	700	700
kw/kg of Pu	-	2,030	2,030	3,500	3,500

*The uranium-235 constitutes 0.40 × 0.80 = 32% of the total heavy atoms

**Excluding end-pellet hot spot factor

the remaining specimens using measured axial power profiles of the capsule. Constant temperatures and temperature gradients will be maintained by axial and radial repositioning of the capsule in response to total and local power measurements. Three types of observations will be made in each pin: mass transport, isothermal axial migration, and thermal-gradient radial migration. Figure 5-3 is a schematic of the various experiments located in six pins of capsule E3A, and Table V-3 summarizes the design parameters.

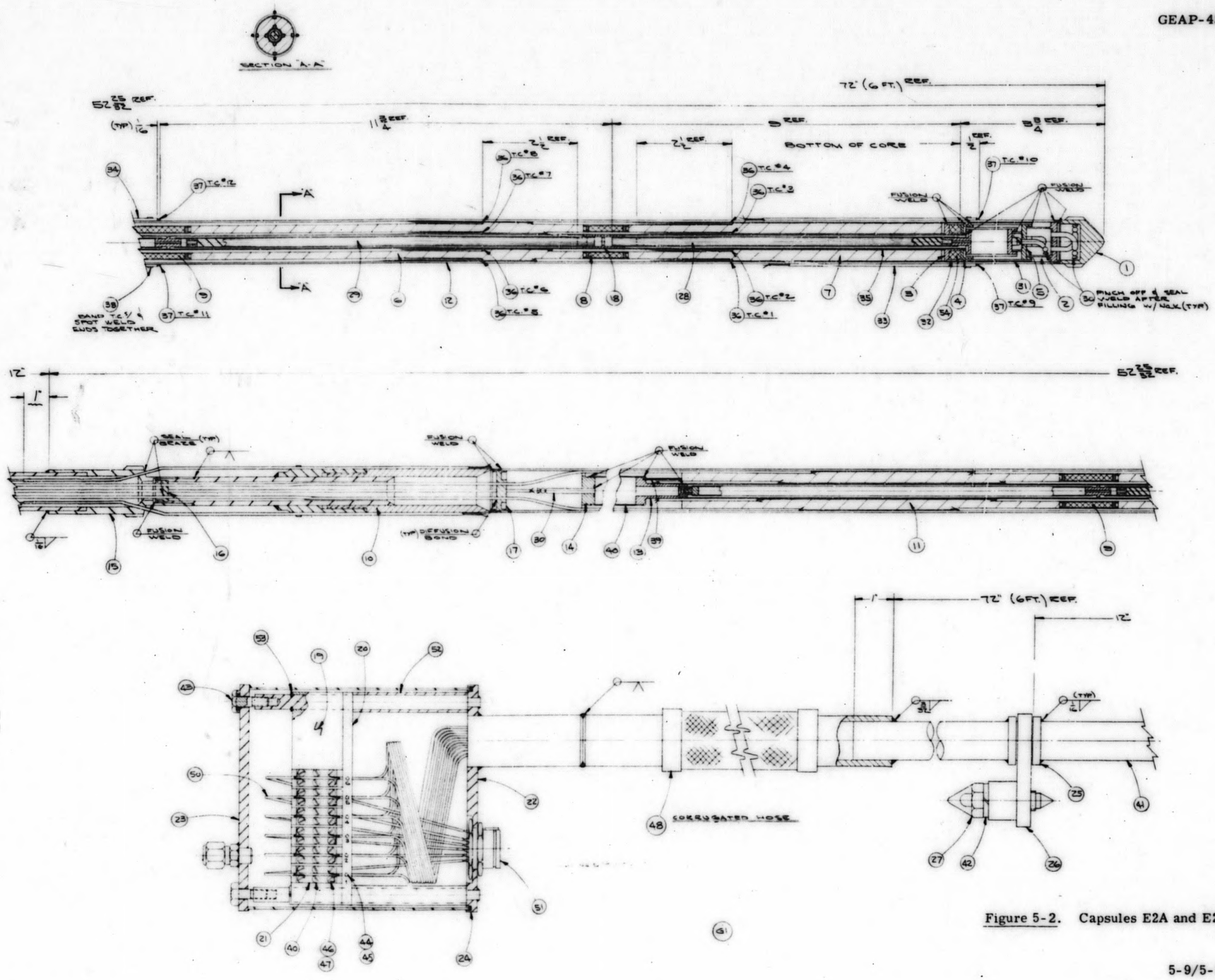

Figure 5-2. Capsules E2A and E2B

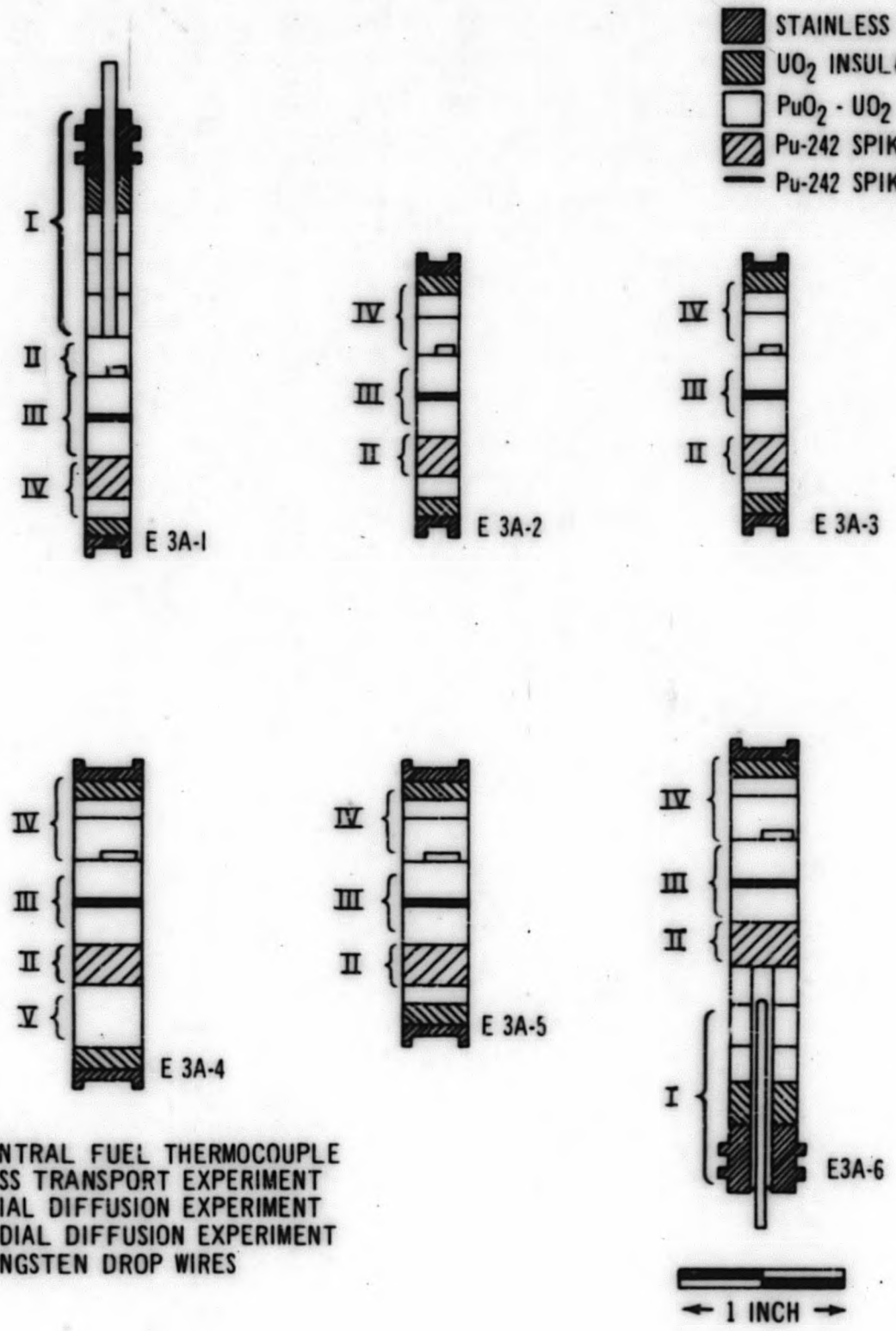

Figure 5-3. Plutonium Migration Specimens

TABLE V-3

E3A PIN DESIGN PARAMETERS

	Specimen Designation							
	1	2	3	4	5	6	7*	8*
Clad OD (inches)	0.250	0.250	0.250	0.375	0.375	0.375	0.250	0.375
Clad thickness (inches)	0.015	0.015	0.015	0.015	0.015	0.015	0.015	0.015
Fuel-clad diametral fabrication gap (mils)	1-3	1-3	1-3	5-7**	5-7**	5-7**	1-3	1-3
Clad material SS-type	← 347 →							
Plutonium-uranium in fuel	0.25	0.25	0.25	0.25	0.25	0.25	0.25	0.25
Oxygen-to-metal ratio	2.05 ±0.01	2.00 ±0.005	1.98 ±0.03	2.00 ±0.005	2.10 ±0.03	1.98 ±0.005	2.00 ±0.005	2.00 ±0.005
Over-all specimen length (inches)	3.00	1.75	1.75	2.00	1.75	3.00	1.50	1.50
Active fuel length (inches)	2.125	1.25	1.25	1.50	1.25	2.125	1.00	1.00
Specimen fill gas	argon →							helium
Peak $\int_{T_s}^{T_c} k d\theta$ (w/cm) at $\bar{\sigma} = 9.6 \times 10^{13}$ nv	51	52	52	57	56	54	24	22
Peak linear power generation (kw/ft) at $\bar{\sigma} = 9.6 \times 10^{13}$ nv	26	26	26	37	36	35	12	14
Power variation over cycle - % of peak power	11	9	7	7	17	30	31	51
Maximum clad temperature (°F)	1250	1250	1250	1250	1250	1250	<600	<600

*For isotopic analysis only; no diffusion couples

**Fuel-clad spacer used to insure four-mil minimum gap

Mass Transport

The center-line region of a radial cavity in a mixed-oxide pellet (see Figure 5-3, Pellet II) is spiked with 50-to-100 micrograms of plutonium-242 and uranium-233. An adjacent pellet of similar composition closes off the cavity. The relative rates of plutonium and uranium transport under the influence of the temperature difference across the cavity will be observed.

Axial Plutonium Diffusion

The adjacent surfaces of two adjoining pellets will be enriched with 50-to-100 micrograms of plutonium-242 to provide an axial diffusion couple (III in Figure 5-3). After irradiation, core samples are to be taken perpendicular to the enriched surface to determine plutonium-242 concentrations along isotherms as a function of distance from the original surface. Cores may be taken at different radii from one couple to determine the temperature dependence of diffusion rates. Numerical methods for analysis of the two-dimensional variable-temperature diffusion are being studied.

Radial Plutonium Diffusion

Solid-state diffusion rates in a thermal gradient will be measured by homogeneously spiking a solid pellet with 50-to-100 micrograms of plutonium-242. Power generating pellets will be located on either side of the spiked pellet to minimize axial temperature gradients. Post-irradiation radial core drilling will be used to sample radial plutonium concentration profiles. The pellet will be indexed by tungsten wires embedded in the perimeter to permit locating the spiked region for sampling after irradiation.

Spiking with Plutonium-242

Preliminary experiments have established the feasibility of evaporating controlled thin layers of plutonium-242 onto the end of a mixed oxide fuel pellet.

Natural uranium spiked with uranium-233 tracer has been used in the preliminary work. The uranium oxide is evaporated in-vacuo from a hot tungsten ribbon filament.

a. The optimum conditions of time, temperature and filament loading to prepare reproducible deposits have been determined.

b. The uniformity of the deposits has been determined autoradiographically. The maximum variation in uniformity from the center to the periphery of the deposit was ±15 percent.

c. Contamination of the deposits by filament material has been investigated using neutron-activated filaments. The contamination amounted to about five percent by weight of a 10 $\mu g/cm^2$ deposit and there was little difference in this respect between tungsten and rhenium filaments, although with unloaded filaments, tungsten transport was about twice as great as rhenium transport.

d. The relative volatilities of plutonium and uranium oxides in a mixture have been examined. Complete evaporation of the filament loading is required, if the initial plutonium-uranium ratio is to be preserved. Initial stages of evaporation show a low plutonium-uranium ratio in the deposited material.

e. Methods for recovering excess plutonium-242 by shrouding the filament, and for determining the thickness and unformity of the deposits, have been developed.

Experiments on flashing of UO_2 - PuO_2 onto the inside surface of an aluminum tube have been unsuccessful due to filament wire bowing. The requirement for radial deposition has been superseded by use of a homogeneously-spiked pellet for measurement of thermal gradient solid state radial diffusion.

Capsule Design

Design calculations are underway to replace the segmented thermal barriers and insulators in the concept drawings of capsule E3A with thermal barriers that are continuous over the length of at least three fuel pin specimens.

Investigations are underway to minimize the effect of flux peaking at the end of each fuel pin. This flux peaking may affect the temperature distributions in the mass transport experiment. Tentative solutions to this problem: (1) bring the active fuel portion of adjacent pins as close together as possible, and (2) provide a constant linear macroscopic cross section with neutron absorbers. The design has active fuel pellets spaced 1/2 inch apart between adjacent fuel pins. The preferred alternate now being evaluated is to observe mass transport in a radial rather than an axial-cavity, eliminating the effect of the flux peak.

Ultrasonic Core-Drilling

Specially shaped drilling bits for ultrasonic core-drilling investigation have been designed and machined. These are required for post-irradiation sampling of the diffusion couples. A series of drilling tests in UO_2 and Al_2O_3 have been done using the available Mullard ultrasonic head. Arrangements have been made to perform some tests with a Raytheon ultrasonic unit.

A core sample of UO_2 approximately 0.014 inch in diameter by 0.070 inch long has been made by ultrasonic drilling. After removal of the bit, the sample remained fixed to the base material. Figure 5-4 shows photographs of the sample in the base material and of the core removed from the base material. In the removal operation the core was broken into two pieces. A sample mounting procedure similar to that used in sectioning semiconductor crystals is being developed to avoid the problem of core detachment from the base material.

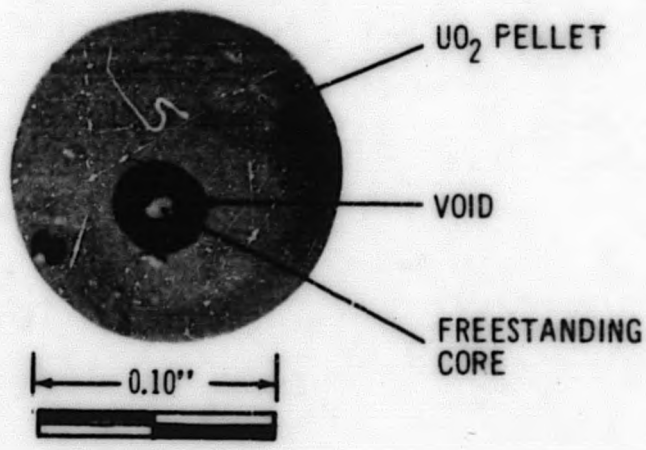

CORE BEFORE REMOVAL

CORE AFTER REMOVAL
(LINE IN LOWER PORTION OF PHOTOGRAPH IS 0.010 IN. DIAMETER WIRE)

Figure 5-4. Core Sample of UO_2 Obtained With Ultrasonic Drill

Preliminary design layout for a remote control stage providing for X-Y-Z motion of the irradiated pellet has been made for accurate positioning in the ultrasonic drilling operation in RML. The drill will initially be installed in the small alpha enclosure, although crowding of equipment will probably make transfer of the drill to a large alpha box desirable when the latter becomes operational early next year.

5.4 Fuel Compositions and Properties: Gravimetric Determination of Oxygen/Metal Ratio

The gravimetric method developed for determination of the oxygen-to-metal ratio in mixed oxides has been adopted as a routine analytical procedure. Approximately 100 unirradiated fuel samples were analyzed during the quarter, most of which are reported in Section 5.5.

A report, GEAP-4271, "The Measurement of Oxygen to Metal Radio in Solid Solutions of Uranium and Plutonium Dioxides", has been prepared for publication.

Consideration is being given to micro-thermogravimetric equipment to permit the analysis of one to ten mg samples of irradiated mixed oxide fuels outside of massive shielding.

5.5 Experimental Fuel Fabrication

5.5.1 Control of Fuel Stoichiometry

Study has continued on the control of mixed-oxide fuel pellet stoichiometry during sintering. It has been observed that when a 7 cfh flow of the 6 percent H_2-94 percent He furnace gas is bubbled through water before entering the furnace, the mixed oxide fuel sintered at $\simeq$1600 C has an O/M ratio of 1.995 to 2.000. Analysis of the gas entering the furnace by a C. E. C. Moisture Monitor under these conditions shows greater than 10,000 ppm of water vapor in the furnace atmosphere. Reduction of the water content below 10,000 ppm. by bubbling only part of the 6 percent H_2-94 percent He gas through water, has resulted in sub-stoichiometric oxide. These observations are essentially in agreement with the thermodynamic calculation of the equilibrium concentration of water vapor for reduction of PuO_2 to Pu_2O_3 using

$\Delta F = -RT \ln \left(\frac{P_{H_2O}}{P_{H_2}} \right)$, although a small uncertainty in the value used for

$\Delta F^\circ_{1900\ K}$ (PuO_2) results in a large uncertainty in P_{H_2O}/P_{H_2}.

The observed water vapor content of the sintering furnace atmosphere versus the stoichiometry of the mixed oxide fuel pellets is indicated by the plot shown in Figure 5-5.

Tabulations of all sintering runs made during the quarter are given in Table V-4.

TABLE V-4

MIXED OXIDE PELLET SINTERING DATA

Date	Batch	Pellet Numbers	Hydraulic Pressing Press.(psig)(a)	Green Density (% TD)	Fired Density (% TD)	O/M	Gas Condition	Firing Temp (°C) and Time	Comments
4/1	B-22	1-12	100-600	40-54	85-91	2.000 ± 0.001	Wet	1600° 4 hrs.	Pilot run-large taper in dia.
4/2	B-22	13-18	100-600	40-54	90-93.5	2.000 ± 0.001	Wet	1575° 4 hrs.	Pellets in good condition
4/3	B-22	19-30	150-350	43-50	89-91	2.000 ± 0.001	Wet	1575° 4 hrs.	Pellets "hour-glassed"
4/5	B-22	31-60	220	46	90	2.000 ± 0.001	Wet	1575° 4 hrs.	All out of spec.
4/8	B-22	61-72	220	46	88.1	1.998 ± 0.001	Wet & Dry	1575° 4 hrs.	3 hr. dry, 1 hr. wet
4/9	B-22	73-84	220	46	87.7	1.998 ± 0.001	Wet & Dry	1575° 4 hrs.	3 hr. dry, 1 hr. wet
4/11	B-22	85-96	150-200	42.5-45	85-93	1.998 ± 0.001	Wet & Dry	1575° 4 hrs.	3 hr. dry, 1 hr. wet
4/12	B-22a	97-101	125-225	41.1-45.8	96.5-98.5	1.997	Dry	1575° 4 hrs.	Pellets in excellent condition
4/15	B-22a	102-115	230	45.8	97.5	1.998	Dry	1575° 4 hrs.	Pellets in excellent condition
4/17	B-23	1-10	100-500	37.0-52.2	95-97	---	Dry	1575° 4 hrs.	Very similar to B-22a
4/19	B-23	11-15	175-275	44.2-48.1	93-97	1.986	Dry	1575° 4 hrs.	Pellet condition as predicted
4/23	B-23	16-27	225	46	96	1.975	Dry	1575° 4 hrs.	75% yield
4/24	B-23	28-39	225	46	97.1	1.980	Dry	1575° 4 hrs.	84% yield
4/25	B-23	40-80	225	46	96	1.985	Dry	1575° 4 hrs.	90% yield
4/26	B-23	80-136	225	46	95.5	1.981	Dry	1575° 4 hrs.	86% yield
4/29	B-24	1-10	100-500	41-53	91-96	1.977	Dry	1575° 4 hrs.	Pilot Run
5/2	B-24	11-16	150-250	43.8-48	96-98	1.976	Dry	1575° 4 hrs.	Confirmation Run
5/6	B-24	17-28	200-225	46 -47.5	--	---	Dry	1575° 4 hrs.	(b)
5/7	B-24	29-40	230	46.8	91	1.995	Dry	1575° 4 hrs.	(c)
5/8	B-24	41-52	230	47.0	97.3	1.972	Dry	1575° 4 hrs.	Normal sintering cycle - pellets in excellent condition
5/9	B-24	53-64	230	46.8	--	---	Dry	1575° 4 hrs.	(d)
5/10	B-24	65-104	230	47	95	1.981	Dry	1575° 4 hrs.	58% yield - diameter problem
5/13	B-24	105-131	230	47	95	1.972	Dry	1575° 4 hrs.	63% yield - diameter problem
5/16	B-25	1-10	100-500	44.5-53.1	95-97	1.990	3700 ppm H_2O	1575° 4 hrs*	Pilot Run- *Temp over-shot temporarily
5/17	B-25	11-21	125-225	45.5-48.2	87.5-96.3	1.985	3000 ppm H_2O	1575° 4 hrs*	Confirmation Run-Temp too low
5/19	B-25	22-33	160	46.6	96.0	1.978	2400 ppm H_2O	1600° 4 hrs.	100% yield
5/21	B-25	34-63	160	46.3	94.1	1.976	3000 ppm H_2O	1600° 4 hrs.	97% yield
5/21	B-26	1-10	100-500	41.3-53.3	92.5-96.5	1.969	2600 ppm H_2O	1600° 4 hrs.	Pilot Run
5/22	B-25	64-91	160	46.0	95.0	1.973	1700 ppm H_2O	1600° 4 hrs.	88% yield-5 annular pellets made
5/23	B-26	11-20	175-250	45.5-48	97.3-98	1.975	1380 ppm H_2O	1600° 4 hrs.	Confirmation Run - 80% yield
5/24	B-25	92-125	160	45.8	94.4	1.973	1860 ppm H_2O	1600° 4 hrs.	94% yield
5/27	B-26	21-50	200	46.5	95.5	1.971	--	1600° 4 hrs.	100% yield
5/29	B-26	51-100	200	46.3-48.3	93.7	1.979	2400 ppm H_2O	1600° 4 hrs.	70% yield
5/31	B-26	101-132	200	46.2-46.5	94.5	1.997	2400 ppm H_2O	1600° 4 hrs.	72% yield
6/5	B-27	1-11	100-500	42.7-57.6	92.7-96.5	1.998	10,00 ppm H_2O	1600° 4 hrs.	Boat in more slowly
6/6	B-27	12-21	160-210	47.5-48.9	96.4-97.0	1.992	--	1600° 4 hrs.	Confirmation Run
6/7	B-28	1-10	100-400	41.7-52.4	93.7-97.5	1.992	--	1600° 4 hrs.	Pilot Run
6/8	B-27	22-51	185	48.3-51.8	95.1-96.3	1.998	10,000 ppm H_2O	1600° 4 hrs.	Diameters too large
6/10	B-28	11-21	160-210	46.2-48.3	96.9-97.6	(e)	(f)	1600° 4 hrs.	Ave Density over 97%
6/11	B-27	52-62	150-175	46.8-47.9	93.8-95.6	1.997	(f)	1600° 4 hrs.	Second Conf. Run
6/12	B-28	22-28	170-210	47.0-48.7	95.1-96.2	(e)	(f)	1600° 3 hrs.	Good Dia. - #21-25
6/13	B-27	63-92	150-155	46.3-48.1	93.8-95.3	1.989	(f)	1600° 4 hrs.	Small Diameter Problem
6/14	B-28	29-68	175-180	46.2-46.8	95.1-97.2	(e)	(f)	1600° 2½ hrs.	Small Diameter Problem
6/15	B-27	93-113	155-168	46.2-47.3	94.3-95.6	1.990	(f)	1600° 4 hrs.	16 Task B Pellets
6/17	B-28	69-96	185-195	46.6-47.4	95.9-97.4	(e)	(f)	1600° 2½ hrs.	Small Diameters
6/20	B-20	1-11	100-500	39.7-54.7	93.3-97.4	(e)	(f)	1600° 2½ hrs.	Pilot Run
6/21	B-28	96-131	190-195	46.1-47.4	92.1-96	(e)	(g)	1600° 2 hrs.	16 Task B Pellets
6/24	B-29	12-21	160-210	45.7-47.1	--	--	(g)	1600° 2 hrs.	Most pellets split
6/25	B-29	32-43	170-200	47.2	95.8-97.1	(e)	(g)	1600° 2½ hrs.	2nd confirmation run

Notes

(a) Hydraulic pressure times factor 85 gives psi on pellet.
(b) Furnace did not reach sintering temperature due to shutdown for moisture meter installation - pellets left in hot zone at 1100°C over week-end - all pellets broken in half and low density.
(c) Pellets over-sintered - left in hot zone over-night.
(d) All pellets broken in half - result of too rapid a heating rate.
(e) O/M analysis not completed.
(f) Only part of furnace gas bubbled through water.
(g) 7 cfh bubbled through water.

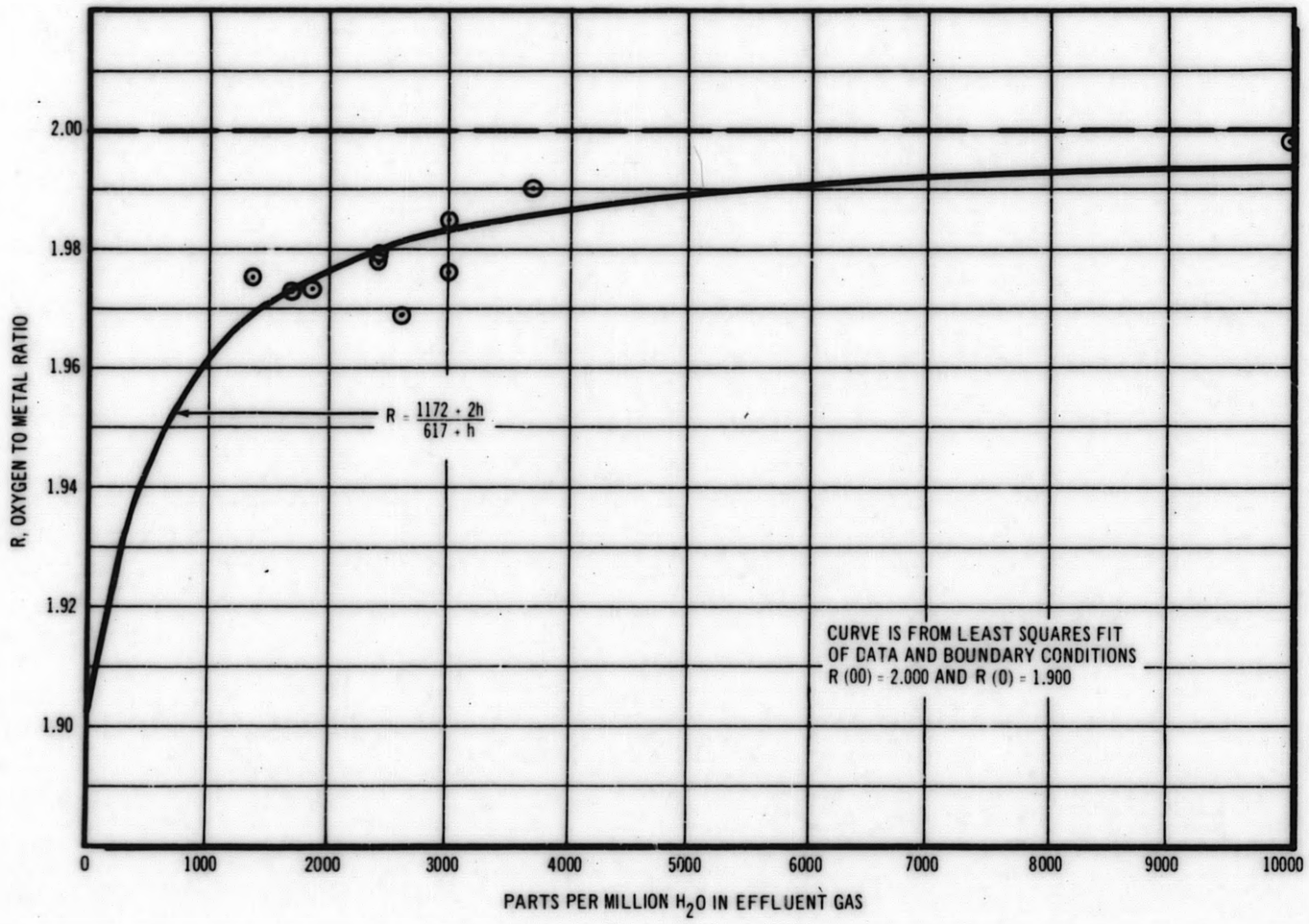

Figure 5-5. Observed Water Content of Sintering Atmosphere vs. Stoichiometry of 80 Percent UO_2 - 20 Percent PuO_2 Pellets

It was observed that when dry gas was used following the use of wet gas, the stoichiometry did not immediately follow as expected. This indicates that the furnace had become saturated with water and could not be quickly dried.

A post-sintering treatment has been used successfully to adjust the stoichiometry of pellet batches which initially were oxygen deficient. This procedure consists of heating the pellets in air to 700 C for 15 minutes, followed by reduction in a 6 percent H_2 - 94 percent He atmosphere at 700 C for three hours and cooling under this atmosphere.

Sub-stoichiometric mixed-oxide fuel pellets are also desired for use in several specimens scheduled for irradiation. Since the only feasible method of obtaining oxygen-deficient mixed-oxide is by reduction with dry hydrogen at high temperature, a small molybdenum-wound sintering furnace has been constructed and placed in operation. This furnace will be operated with a very dry atmosphere obtained by passing the hydrogen-helium gas mixture through a magnesium perchlorate column.

Super-stoichiometric fuel pellets are also desired. The proposed method for their preparation will involve an additional process step after sintering. Knowing the initial stoichiometry and the kinetics of oxygen take-up in air at ≈700 C, this fuel may be carefully oxidized until a given weight increase has been obtained. A soaking period in an inert atmosphere will then be employed to give a homogeneous distribution of the excess oxygen.

5.5.2 Sintering Time-Cycle Improvement

The sintering furnace idling temperature has been increased from 1080 C to 1600 C, and the rate of heating of the pellets has been reduced in order to reduce both firing cycle time and the thermal shock experienced by the pellets (see Figure 5-6). This change shortens the cycle one hour and improves pellet condition. i.e., gives better diametrical consistency per pellet. There is still significant diametrical variation among the pellets in each firing. Attempts will be made to reduce this variation by increasing the green density.

5.5.3 Melting Point of Mixed Oxides

Work has continued on the development of techniques for determining fuel melting points. Temperatures indicated by the two-color pyrometer have agreed well with the known melting points of platinum and columbium metals. When heating a sample rapidly, however, in the Mendenhall V-type tungsten filament - e.g., from 1500 C to 2500 C in 25 seconds - a temperature differential of 100-200 C may exist between filament and center of sample. It appears, therefore, that heating must be controlled to a slower rate. Containment of the sample within a thin sealed tube of tungsten or rhenium will be investigated to determine whether thermal arrests can be observed at melting. The techniques of fabricating, loading, and heating a 1/16-inch diameter rhenium capsule were demonstrated in a rhenium-fuel compatibility experiment reported in Section 5.1.

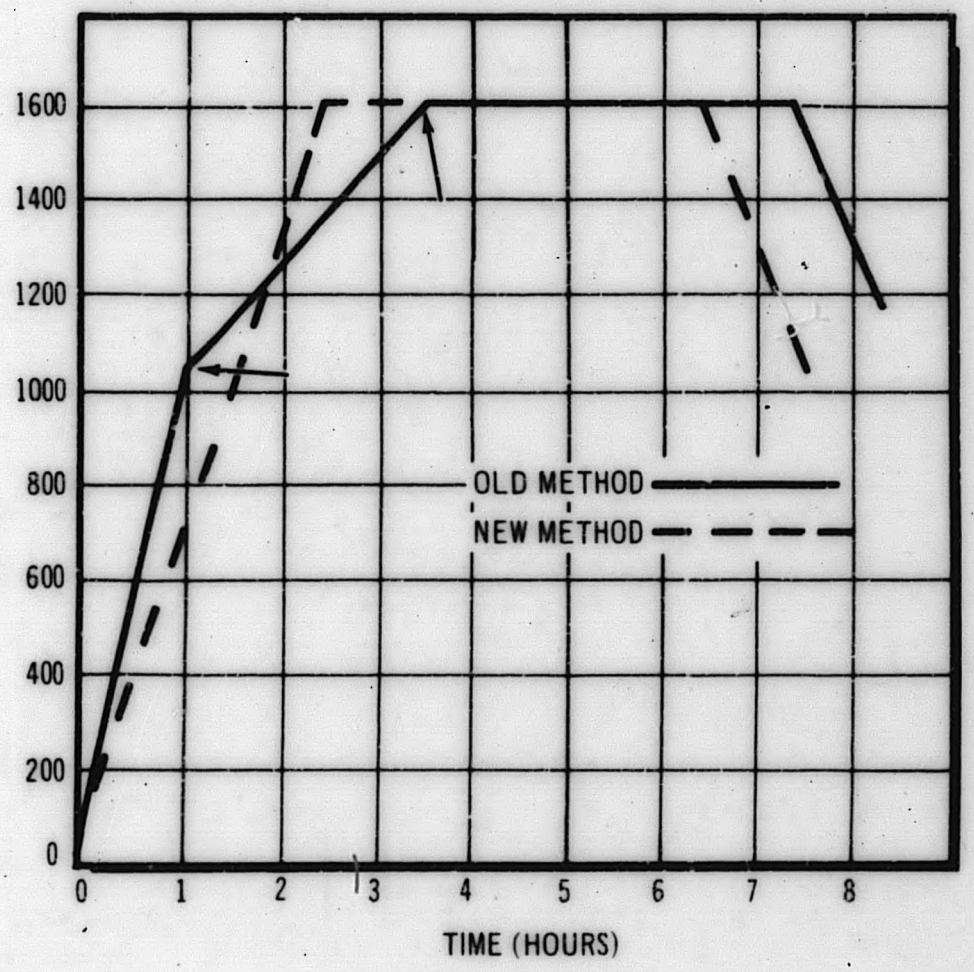

Figure 5-6. Sintering Furnace Cycles

5.5.4 X-Ray Analysis

A preparation technique for handling plutonium-containing samples for X-ray diffraction analysis, which consists of "bagging out" the sample and holder in a thin heat-sealable plastic film, appears to be satisfactory for the safe handling of these samples. The plastics tested, however, have some disadvantages. A one-mil-thick type M Mylar (polyester) film was found to produce an intense diffraction peak between 25 and 27.5 degrees and also some loss in X-ray intensity. A two-mil-thick vinyl film produced only a broad peak of quite low intensity, but a relatively large absorption of the 8.0 kev X-ray beam. Samples of fuel pellets will be submitted for X-ray analysis when the X-ray laboratory ventilation installation has been completed.

Figure 5-7 shows an X-ray fluorescence and diffraction table fitted with a plexiglas fume hood for use with plutonium-containing samples.

Snythetic Fissia

Mixed-oxide prepared from Pr_6O_{11} and UO_2 has been fired in hydrogen atmospheres at 1700 and 1900 C. Preliminary examination indicates incomplete solid solution at 1700 C and probably complete solid solution at 1900 C. Closed capsules with thoria liners have been prepared to permit firings in a closed system so that the O/M ratio will be known from the initial compositions used. Various mixtures of Pr_2O_3, Pr_6O_{11}, UO_2, and $UO_{2.1}$ are being prepared to cover a range of stoichiometries of the mixed-oxides. Materials have been accumulated preparatory to making fissia mixtures simulating 100,000 MWD/T of fuel for properties measurements.

Cladding Materials

Specifications have been prepared and material requests issued to vendors for additional tubing to supplement the Type 347 commercial stock used for FCR pins to date. The candidate tubing materials include the following:

Type 347 vacuum melted
Type 316 vacuum melted
Incoloy-800
Type 304 vacuum melted
Incoloy-800 (modified 0.1 Al max. and 0.1 Ti max.)
Inconel-600 or -625
Ni-O-Nel

These materials will also be used in part for Tasks E and F pin and capsule fabrication to observe behavior in the EBR II capsule environment.

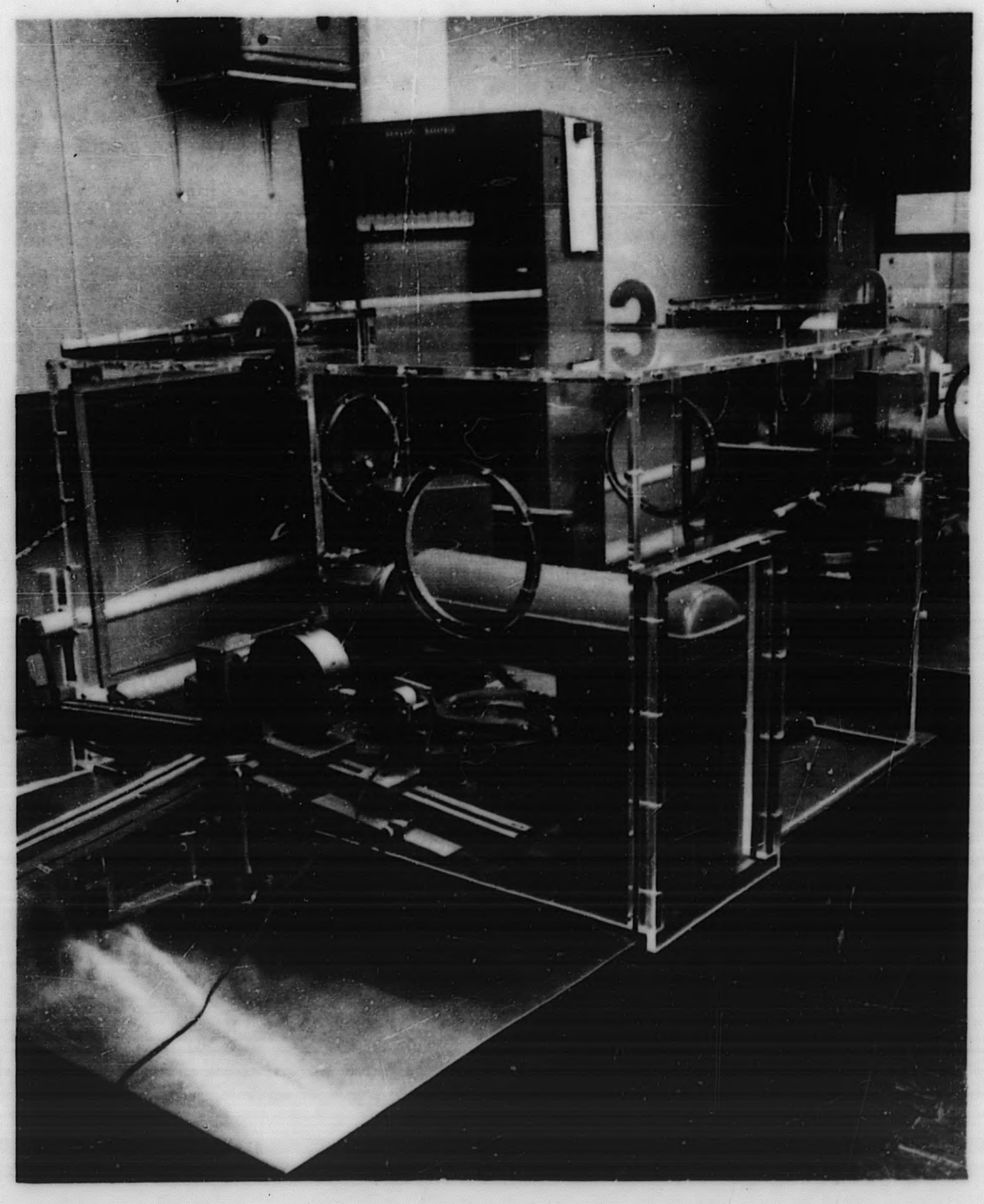

Figure 5-7. X-Ray Fluorescence and Diffraction Table Fitted With A Plexiglas Fume Hood

Plutonium Laboratory Operations

Three shipments of plutonium (ca. 480 grams) and one shipment of fully enriched uranium (2400 grams) were received. A shipment of mixed-oxide scrap containing 108 grams of plutonium and 411 grams of normal uranium was sent to Hanford for recovery.

A dissolver with condenser system was installed in Hood 14 and placed in operation for recovery of mixed-oxide hard scrap. Waste pellets were successfully dissolved and used as feed solution for subsequent mixed-oxide batches. No sintering problems were encountered with this material and pellet yield was normal.

The wet chemistry system, Hood 1, was completely reorganized with the elimination of three vessels and many valves and lines. The resultant simplified system is comparatively trouble-free.

Structural modifications were completed for installation of new pin loading and welding enclosures. New pin loading and welding enclosures were ordered and are scheduled to be received in late July. Installation of these new facilities should be completed by mid-August.

Nuclear Safety Engineering approval was received for new fuel pin loading, decontaminating, and welding facilities and for additional storage cabinets. Each storage cabinet may be divided into one, two, or four separate storage positions; therefore, storage capacity was significantly increased.

Fabrication and installation of a temporary welding fixture for specialized fuel pins was reinitiated. Fixture and necessary hood modifications should be completed by early July.

A new ball mill jar and new balls were placed in operation for milling the 20 percent Pu-32 percent U-235-48 percent U-238 powder for Tasks B and E. Utilization of separate ball mill equipment for 32 percent and 72 percent U-235 powders provides additional assurance of attaining desired U-235 content by eliminating pickup of a heel of different enrichment in the ball mill equipment.

A gas moisture monitoring instrument was installed to permit routine monitoring of inlet and exit sintering furnace gases.

The exhaust filter on Hood 1 was replaced without difficulty or contamination spread. A USAEC team inspected the facility and audited the Source and Special Nuclear Material records and practices. A plastic bag was installed on a Hood 7 glove port to permit material bag-out without movement through other hoods.

SECTION VI

TASK F - FAST FLUX IRRADIATION OF FUEL

6.1 Irradiation in EBR-II

The design of the irradiation test subassembly was revised to conform with the comments received from ANL at the meeting of March 28 and 29, 1963, and was transmitted to ANL. The design was further changed at the May 15, 1963, meeting since the revised subassembly could not be disassembled with EBR-II facilities. In view of the fact that it is not feasible to plan to have equipment to reassemble test subassemblies in the near future, ANL suggested that the subassembly be designed for a single irradiation exposure. Also, since others have requested experimental irradiations, ANL proposed to prepare a test subassembly design for a standardized capsule design. Drawings showing such a design have since been received in an ANL letter of June 21, 1963, for our comment.

The proposed irradiation in EBR-II has been revised based on the expected design of a standard irradiation assembly and consistent with the expected startup of EBR-II This revision was transmitted to ANL in our letter of June 6, 1963. This proposal calls for specimen irradiation in three groups:

Group I. Four encapsulated fuel specimens are to be loaded March 1, 1964, for short-term irradiation at high power. These specimens are intended to obtain information on the safety of irradiating the Group II assembly at high power in EBR-II. This group will consist of the fuel specimen already fabricated and three specimens sectionalized to include some of the parameters of Group II.

Group II. Nineteen encapsulated fuel specimens are to be loaded March 1, 1964, for a target exposure of 100,000 MWD/T. The test subassembly containing these specimens may be loaded initially in the 4th row to accumulate burnup and, assuming favorable results from Group I specimens, it may be transferred to a high power central core position.

Group III. Up to 19 encapsulated specimens or up to 37 fuel pins (without capsules) will be loaded for intermediate term irradiation (20 to 50 thousand MWD/T). This test subassembly will be loaded after examination of Group I specimens (tentatively July, 1964); irradiation of unencapsulated fuel, at that time, would permit a more nearly prototypical test condition of flow, heat transfer, and fuel pin support.

6.1.1. Fuel Test Specimens

In addition to the specimen already fabricated, fuel pellets have been accumulated for approximately seven more specimens. Oxygen-to-metal ratio has not been determined for some pellets and is below specification for others; therefore, a stoichiometry adjustment step is required. A summary of fabricated fuel pellets is presented in Table VI-1.

TABLE VI-1

FABRICATED FUEL PELLETS

Number of Pellets	O/M Ratio	Remarks
93% U-235		
60	1.98 ± 0.005	Adequate for sub-stoichiometric pin.
45	2.00 ± 0.005	
315	1.97 - 1.995	O/M ratio to be adjusted to 2.00. Estimate 80% yield.
40% U-235		
16	1.97 - 1.995	O/M ratio to be adjusted to 2.00. Estimate 80% yield.
69	Unknown	Either 2.00 O/M ratio or to be adjusted to 2.00 with estimated 80% yield.

The above pellets have not been loaded into clad tubing since the change described above has resulted in a shorter specimen.

6.1.2. Capsules and Sodium Filling Equipment

Work on the capsule design has been deferred pending the results of the design change requested by ANL. On the basis that the design will not change the sodium filling method, the fabrication of this equipment has been proceeding.

6.1.3. Hex Tube Assembly

It is expected that this item will be supplied by ANL, described (Section 6.1) as the test subassembly for irradiating standard capsules.

SECTION VII

TASK G - REACTOR DYNAMICS AND DESIGN

7.1 Large FCR Parametric Studies

Parametric studies have been undertaken to evaluate the effects of variations in core composition and geometry on the safety and economic aspects of a large FCR (in the 1000 MWe range). An equivalent bare core model, with 60 energy groups, is being used to compute the uniform sodium temperature coefficient, isothermal Doppler coefficient, core conversion ratio, and total core sodium loss reactivity increment. Bare core perturbation theory is then used to obtain estimates of the nonuniform sodium temperature coefficient and the maximum reactivity increment due to partial or total loss of sodium. For most core compositions chosen, three sets of core dimensions are being evaluated corresponding to diameter-to-height ratios of about 2, 3, and 6. Results of the studies completed to date are given in Table VII-1.

It is seen that the maximum reactivity increment due to partial loss of sodium generally increases with increasing sodium volume fraction, even though the reactivity increment with total loss of sodium may show an opposite trend. Use of a small volume fraction of moderating material significantly reduces the maximum reactivity increment due to partial loss of sodium and appreciably increases the magnitude of the Doppler coefficient. (The U-238 and Pu-239 resonance interaction effect discussed in Section 7.2.2 is not included in the $\left(T \frac{dk}{dT}\right)$ values listed in Table VII-1. Correction for this effect will increase all of the Doppler coefficient values.)

7.2 Doppler Effect Calculations

7.2.1 Multilevel Method Versus Single Level Method For Evaluating Pu-239 Doppler Effect

The infinite dilution fission cross section of Pu-239 ($\bar{\sigma}_f$) and the reduction of the cross section from its infinite dilute values ($\Delta\sigma_f$), due to self-shielding of Doppler-broadened unresolved resonances were calculated using both the multilevel and single level formalisms. This comparison was made for an energy of 1 Kev, a fuel temperature of 300 K, and a potential scattering cross section per absorber atom of 400 barns. Only the l=0, J=1 state was considered. A ν=10 resonance spacing distribution was assumed with an average spacing $\bar{S}$ of 3.33 ev for this Pu-239 state.

The infinite dilute multilevel fission cross section was obtained from the MALD [3] code, and the reduction of the fission cross section due to self-shielding was calculated by using the

MALD output as input to the TEMP [3] code which Doppler-broadens zero temperature cross sections. A random sampling procedure was used with 40 resonances to represent the distributions of neutron width, fission width, and resonance spacing as described in Reference [7].

For the single-level case, the relationships used are those given in Reference [8]:

$$\bar{\sigma}_f = \frac{4.12 \times 10^6 \quad g_J \quad \Gamma_n \cdot \quad \Gamma_f \quad S_f}{E\Gamma \quad S}$$

and

$$\frac{\Delta \sigma_f}{\bar{\sigma}_f} = \frac{2}{T^{\frac{1}{2}}} \quad K(E, \sigma_p):$$

in which

$$K(E, \sigma_p) = \frac{(2.12 \cdot 10^5) \quad (E_x - e)}{E \left[\sigma_p + \frac{507}{E} \right]}$$

Results of the calculations are listed below. The $\bar{\sigma}_f$ values computed with use of the multilevel and single level formalisms agree within about five percent. This agreement is about as good as can be expected in view of the numerical approach utilized in the evaluation with the MALD code. Since the Doppler reactivity effect due to change of the fission cross section is mainly dependent on the fractional change in the cross section, the ratio $\Delta \sigma_f / \bar{\sigma}_f$ is the best single representative of the change due to the Doppler effect. As can be seen from the data below, this ratio does not differ significantly between the two methods. These data indicate that application of multilevel methods in the unresolved resonance region of importance to fast reactor Doppler calculations will not markedly alter results obtained earlier with single-level methods.

	$\bar{\sigma}_f$	$\Delta \sigma_f$	$\Delta \sigma_f / \bar{\sigma}_f$
Multilevel	5.98	0.87	0.145
Single level	5.69	0.84	0.148

7.2.2 Effect of Overlap Between U-238 and Pu-239 Resonances on Doppler Effect

A computer code RAVE, which calculates resonance integrals of Pu-239 and U-238 with the overlap effect recently investigated by Codd and Collins [9], has been programmed on the TRANSAC-2000. This program calculates the Doppler-broadened line shape function $\psi(\xi, x)$ for either resolved resonances or over a Porter-Thomas distribution of resonance widths for

TABLE VII-1

SUMMARY OF 1000 MW(e) PHYSICS SURVEY RESULTS

Case No.	Core Volume Percent				Dimensions in ft. (b)		%Pu 239+241	Core (c) Conversion Ratio	Doppler (d) $T\frac{dk}{dT}$	Sod Coeff $\times 10^6$ $\Delta k/^oC$ (e)		Sod Loss Δk in \$		Six Mos. Oper. React. (g) Δk in \$
	Na	Fuel	Steel	Mod (a)	L	D				Unif.	Non-Unif.	Total	Max.	
PT01	40	30	20	10	2.0	12.5	13.3	0.78	-.0120	2.7	9.0	2.6	4.5	6.6
PT02	40	30	20	10	3.3	9.8	11.8	0.89	-.0143	3.7	11.0	4.1	5.4	4.8
PT03	40	30	20	10	4.3	8.6	11.4	0.92	-.0150	4.3	12.3	4.7	5.8	4.3
PT04	40	35	15	10	1.9	11.9	12.3	0.83	-.0118	3.0	9.8	2.9	4.9	5.6
PT05	40	35	15	10	3.1	9.3	10.9	0.95	-.0140	3.8	11.8	4.3	5.6	3.8
PT06	40	35	15	10	4.1	8.1	10.5	0.99	-.0147	4.5	12.9	4.9	5.9	3.0
PT07	50	25	16.7	8.3	2.1	13.3	14.5	0.72	-.0113	0.85	7.9	-0.1	4.2	7.5
PT08	50	25	16.7	8.3	3.5	10.4	12.5	0.84	-.0140	2.84	12.1	2.8	5.7	5.7
PT09	50	25	16.7	8.3	4.5	9.1	12.0	0.88	-.0149	3.70	13.6	3.9	6.4	4.9
P10A	40	38	20	$2\,ZrH_{1.4}$	1.9	11.5	11.5	0.81	-.0101	--	--	1.0	--	5.9
PT10	40	38	20	2 ZrH	1.9	11.5	11.5	0.81	-.0091	2.0	7.9	1.1	3.9	5.9
PT11	40	38	20	2 ZrH	3.0	9.0	10.1	0.94	-.0111	2.3	9.9	3.0	4.8	3.9
PT12	40	38	20	2 ZrH	4.0	7.9	9.7	0.98	-.0118	3.2	11.1	3.7	5.4	3.3
PT13	50	33.3	16.7	0	1.9	12.1	12.3	0.78	-.0051	1.4	11.7	-0.7	5.2	6.0
PT14	50	33.3	16.7	0	3.2	9.4	10.4	0.96	-.0071	5.1	19.3	3.8	7.5	3.6
PT15	50	33.3	16.7	0	4.1	8.3	10.0	1.01	-.0078	6.6	22.2	5.7	9.1	2.8
PT16	40	35	20	5	1.9	11.9	11.9	0.84	-.0082	2.8	9.5	2.3	4.4	5.4
PT17	40	35	20	5	3.1	9.3	10.5	0.97	-.0104	3.5	11.8	3.9	5.3	3.5
PT18	40	35	20	5	4.1	8.1	10.1	1.02	-.0111	4.1	12.7	4.6	6.0	2.7
PT19	60	20	13.3	6.7	2.3	14.3	16.8	0.63	-.0110	-3.5	3.6	-6.4	3.2	9.0
PT20	60	20	13.3	6.7	3.7	11.2	14.1	0.76	-.0137	1.6	12.3	-1.0	6.0	6.9
PT21	60	20	13.3	6.7	4.9	9.8	13.4	0.81	-.0145			1.0	6.9	6.1
PT22	20	40	26.7	13.3	1.8	11.4	11.7	0.89	-.0128	1.1	3.4	1.5	2.3	4.7
PT23	20	40	26.7	13.3	3.0	8.9	10.7	0.98	-.0146	1.2	3.3	1.8	2.3	3.2
PT24	20	40	26.7	13.3	3.9	7.8	10.5	1.01	-.0152	1.2	3.2	1.9	2.3	2.9
PT25	40	24	16	20	2.2	13.5	14.8	0.73	-.0147	0.2	1.8	1.0	2.5	7.8
PT26	40	24	16	20	3.5	10.5	13.3	0.81	-.0172	0.2	2.4	1.9	2.9	6.2
PT27	40	24	16	20	4.6	9.2	12.9	0.83	-.0179	0.3	2.8	2.3	3.1	5.9
PT28	50	30	17	3 ZrH	2.0	12.5	13.2	0.70	-.0097	-0.9	5.0	-1.5	3.6	7.4
PT29	50	30	17	3 ZrH	3.3	9.8	11.4	0.82	-.0120	1.7	10.1	1.3	5.1	5.6
PT30	50	30	17	3 ZrH	4.3	8.6	10.9	0.86	-.0125	2.6	11.6	2.4	5.6	5.0
PT31	40	36	20	4 ZrH	1.9	11.8	11.9	0.77	-.0113			0.7	3.0	6.3
PT32	40	36	20	4 ZrH	3.1	9.2	10.5	0.87	-.0130			2.3	4.0	4.6
PT33	50	30	16	4 ZrH	2.0	12.5	13.3	0.69	-.0104			-1.5	3.3	7.5
PT34	50	30	16	4 ZrH	3.3	9.8	11.5	0.80	-.0124			1.1	4.7	5.8
PT35	40	32	20	8 ZrH	2.0	12.2	13.8	0.66	-.0117			-0.9	1.8	7.9
PT36	40	32	20	8 ZrH	3.2	9.6	12.2	0.73	-.0131			0.6	2.5	6.2

Notes

(a) The moderator is BeO except where ZrH or $ZrH_{1.4}$ is denoted.

(b) The core volume is obtained in each case by assuming 2500 MWt, 88 percent of which is generated in the core, and a fuel specific power of 125 KWt/kg(U+Pu).

(c) Core conversion ratio refers to Pu(239+241) rate of creation to rate of destruction in core. All physics data are for an equilibrium 100,000 MWD/T cycle averaged over core batches (~50,000 MWD/T condition).

(d) $T\frac{dk}{dT}$ is the isothermal Doppler coefficient multiplied by the absolute temperature (calculated from the reactivity change for a fuel temperature change from 1400 K to 700 K).

(e) Nonuniform sodium coefficient is the reactivity increment for a 1 C rise of sodium temperature at the position of average power density.

(f) "Total" Δk is reactivity gain due to loss of sodium from the entire reactor. Reflector savings is increased 3.75 cm for 60 v/o sodium cases, 3 cm for 50 v/o sodium cases, 2.25 cm for 40 v/o sodium cases, and 1.0 cm for 20 v/o sodium cases when sodium is removed (δ = 20 cm with sodium present).
"Max" Δk is reactivity gain due to complete voidage of sodium in the central region of the core, this region being of such height and diameter as to give the maximum Δk.

(g) The values listed (excess operating reactivity for 6 months between refuelings) are estimates based on the following assumptions:

(1) \$3 is allowed for fission product buildup

(2) Normalize to \$6.6 for Case PT01 since this value was obtained from one-dimensional multigroup calculations on a 24-inch thick reactor core with composition identical to that of Case PT01.

(3) For cases containing appreciable moderating material, excess Δk over \$3 is proportional to one minus "Core Conversion Ratio".

(4) Small reduction of excess Δk is allowed for unmoderated cases, or slightly moderated cases, since higher leakage into blanket for these cases (for equal core conversion ratio) contributes sustaining reactivity.

the unresolved resonance region as presently calculated with the RAPTURE Code. RAVE approximates the Porter-Thomas distributions by calculating fifteen $\psi(\xi, x)$ values for Pu-239, (corresponding to five $\Gamma_n^{(o)}$ and three Γ_f values) and five $\psi(\xi, x)$ values for U-238 (corresponding to five $\Gamma_n^{(o)}$ values).

Shown in Figure 7-1 is a typical plutonium resonance overlapped by two uranium resonances. If the Pu-239 resonance is directly under the U-238 resonance, a rise in temperature will increase the flux near the peak of the Pu-239 resonance since the flux is dominated by the U-238 resonance. Therefore, the Pu-239 effective resonance integral will increase irrespective of its own Doppler broadening.

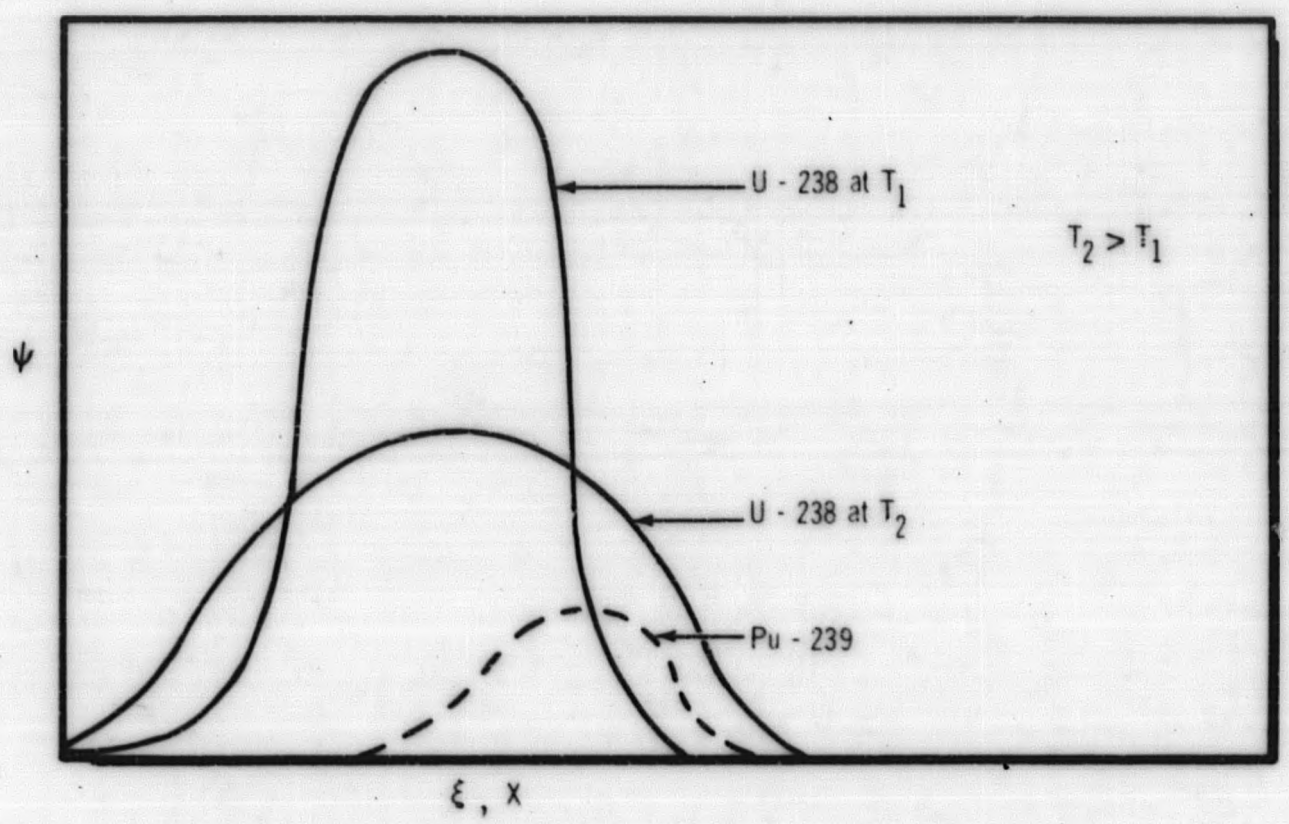

Figure 7-1. Typical Plutonium - Uranium Resonance Overlap

If the Pu-239 resonance is somewhere on the wings of the U-238 resonance, an increase in temperature will decrease the flux and, hence, decrease the absorption in the Pu-239 resonance.

The basic equation used in calculating the plutonium resonance integrals is:

$$I_a^{Pu} = \frac{\sigma_p (\Gamma_\gamma + \Gamma_f)}{2} \int_{-\infty}^{+\infty} \frac{\psi^{Pu}}{\psi^{Pu} + \beta + R\psi^{U}} dx$$

in which:

$$R = \frac{N^U}{N^{Pu}} \cdot \frac{\sigma_o^U}{\sigma_o^{Pu}}$$

Calculations of the Pu-239 effective resonance integral, I_a, for random spacing between Pu-239 and U-238 resonances for an FCR design (see Table 18 of Reference 8) using the RAVE code have been made at two energy levels (1 and 10 Kev). Also ΔI_a, the change of the resonance integral due to an increase in fuel temperature, was computed at these energies. Results of these calculations are listed below in Table VII-2.

TABLE VII-2

CALCULATED Pu-239 EFFECTIVE RESONANCE INTEGRAL

Energy	Temp. °K	Temp. Rise °K		I_a		ΔI_a	
				Overlap	No Overlap	Overlap	No Overlap
1 Kev	1000			22.4	26.6		
1 Kev	2250			22.4	27.1		
1 Kev		1000	2250			+0.01	+0.50
10 Kev	700			5.92	6.23		
10 Kev	1400			5.92	6.24		
10 Kev		700	1400			-0.005	+0.015

This indicates that the overlap of the U-238 and Pu-239 resonances greatly reduces the positive Pu-239 contributions to the Doppler effect and may even render a negative contribution at some energies.

7.3 Code Development for Cross Section Generation

7.3.1 IVAN and SPEC Computer Codes

Composition-dependent multigroup cross section sets for the parametric studies described in Section 7.1 were calculated utilizing a computer code called IVAN. Equations were set up to calculate group-dependent ζ_p (potential scattering per absorber atom) values for U-238, Pu-239 and Pu-240 from atom densities specified as input. These material and group-dependent σ_p values are then used to calculate:

$$\sigma_{n,\,i} = a_{n,\,i} + (b\,\sigma_p)_{n,\,i} + (c\,\sigma_p^2)_{n,\,i} + (d\,\sigma_p^3)_{n,\,i}$$

$$\Delta\sigma_{n,\,i} = -\exp\left[A_{n,\,i} + (B\,\sigma_p)_{n,\,i} + (C\,\sigma_p^2)_{n,\,i} + (D\,\sigma_p^3)_{n,\,i}\right]$$

in which:

$\sigma_{n,\,i}$ is the capture or fission cross-section for material n in group i at a fuel temperature of 1400 K.

$\Delta\sigma_{n,\,i}$ is the change, due to the Doppler effect, in capture or fission cross section for material n in group i for a temperature change from 700 K to 1400 K.

and the coefficients (a, b, c, d, A, B, C, D) were obtained from a least-square fit.

A new code SPEC has been written to further automate and simplify the obtaining of composition-dependent multigroup cross sections. SPEC performs the IVAN computations described above and, in addition, provides cards which may be used as input for the MISY multigroup calculations.

7.3.2 TRAN and EICA Computer Codes

Programming of the computer code TRAN has been completed and most of the routines have been checked out. TRAN will generate a fine group cross section file for use in EICA.

EICA is a zero-dimensional code which will utilize the TRAN file to generate an appropriately averaged set of multigroup cross sections for use in one- or two-dimensional diffusion theory calculations. The EICA code has been specified and programming is about 50 percent complete.

7.4 Reactor Safety and Dynamics

A continuing effort is being carried out to evaluate significance and interaction of the Doppler and sodium reactivity coefficients in reactor safety and transient performance.

In relation to the sodium reactivity coefficient, the hydraulic, thermal, and mechanical design of the core is relevant. An adequate evaluation of the effects of the sodium coefficient during damaging accidents requires that the rate at which coolant can be safely lost due to vaporization be defined. It is planned to develop a modification of the FORE computer program which will take into account coolant vaporization effects.

The influence of the Doppler effect in the core disassembly process following a meltdown accident has been examined with a Bethe-Tait type model in which the Doppler effect as well as

core disassembly is considered in the reactor shutdown process. By means of a computer program parametric studies have been performed to evaluate the influence of the Doppler effect as a function of other key parameters.

In the calculations the power excursion and reactor shutdown are followed, starting at the time that a threshold energy density, Q*, is achieved at the core center and the reactor is above prompt critical by an excess reactivity, k_{ex}. As in the standard Bethe-Tait treatment pressures tending toward disassembly are assumed proportional to the increased energy density above Q*. The Doppler effect is taken to have either a T^{-1} or a $T^{-3/2}$ temperature dependence. The reactor power, Doppler reactivity, and the reactivity reduction produced by disassembly are all followed in time. In principle, the treatment is similar to that of Nicholson [12] except that the strict threshold assumption of the Bethe-Tait model is retained. This produces a somewhat conservative (i. e., high) value for the energy release, but permits a separation of the effects of the key parameters and a better understanding of the results. In addition, the threshold assumption makes possible the integration over the core of the energy density above Q*, an the interpretation of this energy, Ew, as the maximum energy available for (explosive) work.

The Doppler effect reduces the dependence on neutron lifetime of the energy release above threshold. In the case of a constant reactivity insertion rate in the presence of a strong Doppler coefficient, the energy release is reduced as the neutron lifetime is decreased.

As a quantitative example of the use of the method, the worst hypothetical accident described in the Fermi hazards report is recalculated as a function of the Doppler effect. Energy releases, Ew, are reduced from 650 pounds maximum equivalent explosive energy with no Doppler effect to about 22 pounds maximum equivalent energy, in the case in which $T(dk/dT)_{Doppler} = 0.01$ at the melting point and there is a T^{-1} Doppler dependence. If a $T^{-3/2}$ temperature dependence is assumed, Ew is raised to 28 pounds equivalent explosive energy release under the same conditions.

REFERENCES

1. Bell, J., Uranium Dioxide Properties and Nuclear Applications, USAEC, July, 1961, pg. 251.

2. Anderson, J. S. and Sawyer, J. O., Dissociation of UO_2 at its Melting Point, Nature, March 26, 1960, pg. 915.

3. Sixth Quarterly Report, Fast Ceramic Reactor Development Program, January-March, 1963, GEAP-4214.

4. Field, J. H., Experimental Studies of Transient Effects in Fast Reactor Fuels, Series I, UO_2 Irradiations, GEAP-4130, November 15, 1962.

5. Ceramics Research and Development Operation Quarterly Report, October - December, 1962, HW-76300.

6. Lyons, M. F., et al., UO_2 Fuel Rod Operation with Gross Central Melting, ANS paper presented at the 1963 Annual Meeting, Salt Lake City, June 17-19, 1963.

7. Ferziger, J. H., Greebler, P., Kelley, M. D., and Walton, J. W., Resonance Integral Calculations for Evaluation of Doppler Coefficients - The RAPTURE Code, GEAP-3923, July, 1962.

8. Greebler, P. and Goldman, E., Doppler Calculation for Large Fast Ceramic Reactors, GEAP-4092, December, 1962.

9. Codd, J. and Collins, J. P., Plutonium-239 and Uranium-238 Resonance Interaction Effects in a Dilute Fast Reactor, E. A. E. S. - Symposium on "Advances in Reactor Theory", Karlsruhe, April 23-23, 1963.

10. Nicholson, R. B., Methods for Determining the Energy Release in Hypothetical Reactor Meltdown Accidents, APDA - 150, December, 1962.

ACKNOWLEDGMENT

The Fast Ceramic Reactor Development project is being conducted by the General Electric Company with the following personnel contributing to the project during the seventh quarter.

Project Engineer	K. P. Cohen F. J. Leitz
Vented Fuel Development	G. L. O'Neill W. Bailey J. Boyden R. Hess M. Johnson L. Miller
Fuel Testing in TREAT	J. H. Field J. Gilbertson
Fuel Performance Evaluation	E. L. Zebroski D. P. Hines P. E. Novak
Fast Flux Irradiation Testing	W. W. Kendall R. Beggs
Reactor Dynamics and Design Evaluation	P. Greebler D. B. Sherer C. L. Allen N. Friedman B. A. Hutchins R. Protsik W. Sangster J. Sueoka
Irradiation Services - Program Engineer	S. L. Mitchell
Plutonium Fuel Fabrication Laboratory	H. W. Alter
Experimental Studies	W. L. Lyon J. L. Bennett W. M. Cavanaugh

Operation and Fabrication	E. F. Kurtz T. H. Kopper T. E. Lannin T. E. Ludlow R. A. Manchen D. S. Shields M. C. Thompson
Equipment Engineering	J. E. Hanson
Radioactive Materials Laboratory	S. C. Furman R. W. Darmitzel
Metallurgy and Ceramics	L. N. Grossman A. I. Kaznoff M. B. Reynolds M. J. Sanderson
Chemistry and Chemical Engineering	D. H. Ahmann L. F. Epstein
Fuels and Materials Development	R. F. Kirby J. T. Mommsen C. N. Spalaris

END